Published in final edited form as:

Cell Stem Cell. 2020 May 07; 26(5): 707–721.e5. doi:10.1016/j.stem.2020.03.004.

Mosaic mutant analysis identifies PDGFRα/PDGFRβ as negative regulators of adipogenesis

Chengyi Sun[1,2,6], **Hiromi Sakashita**[1,6], **Jang Kim**[1], **Zifeng Tang**[1], **G. Michael Upchurch**[1,3], **Longbiao Yao**[1], **William L. Berry**[4], **Timothy M. Griffin**[5], **Lorin E. Olson**[1,7,*]

[1]Cardiovascular Biology Research Program, Oklahoma Medical Research Foundation, Oklahoma City, OK 73104, USA

[2]Division of Molecular Cardiovascular Biology, Cincinnati Children's Hospital Medical Center, Cincinnati, OH 45229, USA

[3]Department of Pathology and Immunology, Washington University School of Medicine, St. Louis, MO 63110, USA

[4]Department of Surgery, University of Oklahoma Health Sciences Center, Oklahoma City, OK 73104, USA

[5]Aging and Metabolism Research Program, Oklahoma Medical Research Foundation, Oklahoma City, OK 73104, USA

SUMMARY

Adipocyte progenitors (APs) express platelet-derived growth factor receptors, PDGFRα and PDGFRβ. Elevated PDGFRα signaling inhibits adipogenesis and promotes fibrosis, however the function of PDGFRs in APs remains unclear. We combined lineage tracing and functional analyses in a sequential dual-recombinase approach that creates mosaic *Pdgfr*-mutant cells by Cre/lox recombination with a linked Flp/frt reporter to track individual cell fates. Using mosaic lineage labeling, we show that adipocytes are derived from the *Pdgfra* lineage during postnatal growth and adulthood. In contrast, adipocytes are only derived from the mosaic *Pdgfrb* lineage during postnatal growth. Functionally, postnatal mosaic deletion of PDGFRα enhances adipogenesis and adult deletion enhances β3-adrenergic receptor induced beige adipocyte formation. Mosaic deletion of PDGFRβ also enhances white, brown and beige adipogenesis. These data show both

*Correspondence to: Lorin E. Olson, Lorin-Olson@omrf.org, phone: 405-271-7535.

[6]These authors contributed equally

AUTHOR CONTRIBUTIONS

C.S., H.S., and L.E.O. designed experiments and analyzed data. C.S., H.S., J.K., T.T., W.L.B, L.Y., G.M.U., and L.E.O. performed experiments. C.S., H.S., and L.E.O. wrote the manuscript. C.S., H.S., T.M.G., and L.E.O. edited the manuscript. Co-first authorship of C.S. and H.S. is equal, and this citation will be listed with the alternative author orders in the author's curriculum vitae and bibliographies.

[7]Lead Contact

COMPETING FINANCIAL INTERESTS

The authors declare no competing or financial interests.

PDGFRs are cell-autonomous inhibitors of adipocyte differentiation and implicate downregulation of PDGF signaling as a critical event in the transition from AP to adipocyte.

Graphical Abstract

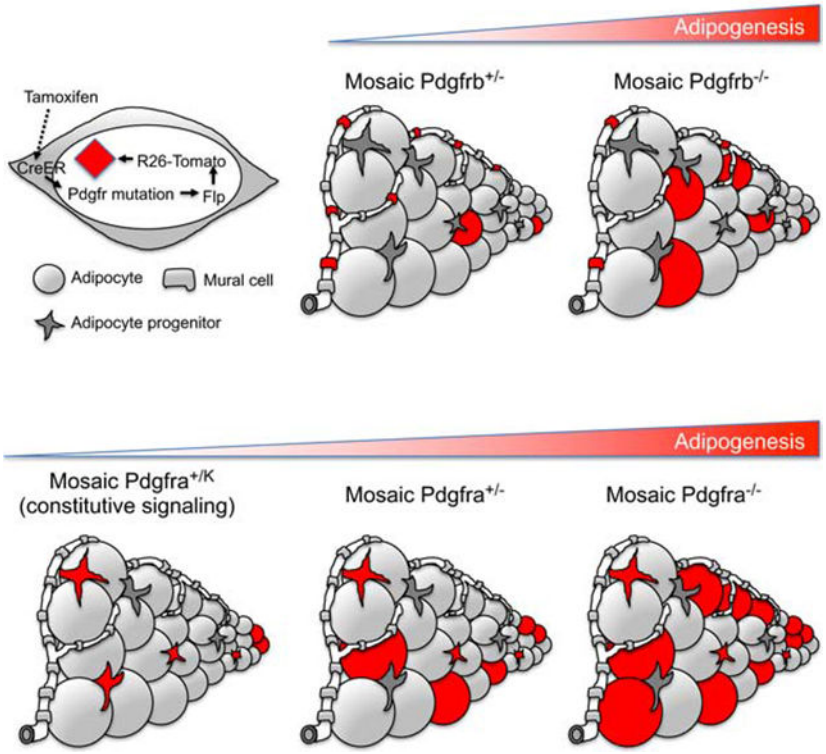

eTOC Blurb

Platelet-derived growth factor receptors are markers for adult mesenchymal progenitor cells. Olson et al. analyze mice with induced functional genetic mosaicism for *Pdgfra* or *Pdgfrb* and demonstrate that both receptors cell-autonomously inhibit adipocyte differentiation, which implicates downregulation of PDGF signaling as a critical event in adipogenesis.

INTRODUCTION

Adipocyte progenitors (APs) are a mesenchymal cell type that resides in connective tissues throughout the body with potential to differentiate into different kinds of adipocytes or myofibroblasts. White adipocytes (WAs) are specialized to store lipid. Brown and beige adipocytes (BAs and bAs) convert lipid stores into heat. Platelet-derived growth factor (PDGF) receptors PDGFRα and PDGFRβ are markers for APs, but they are also expressed on other cells. PDGFRα is expressed in embryonic neural crest and mesoderm and remains highly expressed in many adult fibroblastic cells and mesenchymal progenitors. PDGFRβ is expressed in some of the same embryonic and adult cells as PDGFRα, and also highly expressed in mural cells including vascular smooth muscle cells (VSMCs) and pericytes (Andrae et al., 2008; Armulik et al., 2011; Hoch and Soriano, 2003). Several questions remain about PDGFR expression in APs, as different studies have emphasized one receptor

or the other as an AP marker. There is agreement that the *Pdgfra*-lineage includes most or all types of APs (Berry and Rodeheffer, 2013; Gao et al., 2018; Lee et al., 2015; Lee et al., 2012). In contrast, studies of the *Pdgfrb*-lineage reached different conclusions. The first study to implicate PDGFRβ in the adipocyte lineage used *Pdgfrb-Cre*^{tg} to label WAs from development through postnatal day 30 (P30) (Tang et al., 2008). Since PDGFRβ is a well-known marker for mural cells, this aligns with the expectation that blood vessels are a niche for APs (Nishimura et al., 2007). However, a different *Pdgfrb-Cre*^{tg} did not label WAs in development or in young mice and only labeled them in mice older than 8 weeks of age (Gao et al., 2018). Inducible systems have also been tested: tamoxifen-inducible *Pdgfrb-CreER*^{tg} labeled embryonic APs (Hong et al., 2015), and a doxycycline inducible *Pdgfrb-rtTA;TRE-Cre* approach labeled adult WAs in response to long-term high fat diet (HFD) (Vishvanath et al., 2016). The *Pdgfrb*-lineage studies have all used different transgenes for lineage tracing, which may underlie different results. Single-cell RNA sequencing has emphasized that APs are heterogeneous and may express both PDGFRs (Burl et al., 2018; Hepler et al., 2018; Merrick et al., 2019; Schwalie et al., 2018). A parallel comparison of the *Pdgfra*- and *Pdgfrb*-lineages using a consistent genetic approach would improve understanding of AP identity.

Aside from *Pdgfr* expression and lineage analysis, an important question relates to the *in vivo* function of PDGFRs in mesenchymal progenitors. PDGF regulates cell proliferation, migration, and differentiation by binding to its receptors. This leads to dimerization and autophosphorylation on tyrosine residues in the cytoplasmic domain, which triggers recruitment of kinases and adaptor proteins that activate downstream signaling pathways (Heldin and Westermark, 1999). Gain-of-function mutation of mouse PDGFRα causes APs to become myofibroblast-like cells that secrete ECM and generate fibrosis in adipose tissue (Iwayama et al., 2015). A similar mutation in mouse PDGFRβ also causes adipose tissue fibrosis in some contexts (He et al., 2017). It is not clear if PDGF signaling blocks adipogenesis cell-autonomously by inhibiting AP differentiation into fat cells or indirectly via production of profibrotic ECM. It is intriguing that PDGFRs are downregulated during adipocyte differentiation as this may suggest an important function for PDGFR in the transition from progenitor to mature adipocyte. It remains to be tested whether PDGFR loss-of-function might increase adipogenesis.

The complicated expression pattern of PDGFRα/PDGFRβ and the potential for confounding cell non-autonomous effects (like fibrosis) make delineation of *in vivo* functions very challenging. Here, we created new conditional knockin mice that allow Cre/lox-mediated mutation of *Pdgfra* or *Pdgfrb* with genetically linked Flp/frt-mediated lineage labeling. This dual-recombinase system labels single mutant cells and their progeny with a fluorescent reporter. Utilizing this system, we perform lineage labeling to compare the adipogenic potential of the *Pdgfra* and *Pdgfrb* cell lineages during embryonic, postnatal, and young adult growth. We also used this system to perform mosaic mutant analysis, which allowed us to investigate the *in vivo* function of PDGFRα/PDGFRβ in adipogenesis across different fat depots while minimizing confounding indirect effects of widespread mutation.

RESULTS

Characterization of Conditional PDGFR-Flp Knockin Mice

The genetic mosaic approach generates mutations in a few scattered cells while leaving most cells in the tissue unchanged. For this to succeed, it is crucial to unambiguously distinguish rare mutant cells from non-mutant cells. To ensure that only mutant cells acquire a lineage label, we generated mice to combine the Cre/lox and Flp/frt recombination systems in a sequential dual-recombinase approach. Here, Cre is used to create mutations and permit expression of an optimized Flp recombinase (Flp^o) (Raymond and Soriano, 2007) from the mutant allele, which activates a Tomato reporter (Fig. 1a). This configuration creates a genetic link between gene mutation and cell labeling. Here we describe three new knockin alleles. The *Pdgfra* conditional loss-of-function allele is called aR-Flp and expresses PDGFRα protein; following Cre recombination it becomes aR-ΔFlp and expresses Flp^o (Fig. 1a'). Similarly, the *Pdgfrb* conditional loss-of-function allele, called bR-Flp, switches from PDGFRβ expression to Flp^o expression (bR-ΔFlp; Fig. 1a''). The *Pdgfra* conditional gain-of-function allele, called aR-K.Flp, is silent in the absence of Cre, and switches to express $PDGFR\alpha^K$ and Flp^o following Cre recombination (Fig. 1a'''). K denotes constitutively active $PDGFR\alpha^K$, which has a D842V mutation in the kinase domain (Heinrich et al., 2003; Olson and Soriano, 2009). See Supplementary Figure 1 and the Methods section for detailed information regarding targeting vectors. Correctly targeted ES cell clones were used to generate chimeras for germline transmission of the knockin alleles.

Cre-naïve $Pdgfra^{Flp/Flp}$ ($aR^{Flp/Flp}$), $Pdgfrb^{Flp/Flp}$ ($bR^{Flp/Flp}$), and $Pdgfra^{K.Flp/+}$ ($aR^{K.Flp/+}$) mice were viable and phenotypically normal. They expressed PDGFR proteins at a level similar to wild type or slightly reduced in the case of $aR^{K.Flp/+}$ (Supplementary Fig. 2a-c). This indicates that PDGFRα and PDGFRβ cDNA knockins can substitute for the endogenous *Pdgfra* and *Pdgfrb* genes in most situations (Klinghoffer et al., 2001). *Sox2-Cre*^{tg} expresses Cre in the epiblast and globally targets all cell lineages including the germline. By crossing *Sox2-Cre* with $aR^{Flp/Flp}$ or $bR^{Flp/Flp}$ mice, we generated $aR^{\Delta Flp/+}$*;Sox2-Cre* and $bR^{\Delta Flp/+}$*;Sox2-Cre* mice where one *Pdgfr* allele is replaced by Flp (Supplementary Fig. 2d,e). Backcrossing resulted in $aR^{\Delta Flp/\Delta Flp}$ or $bR^{\Delta Flp/\Delta Flp}$ embryos that do not survive (Soriano, 1994, 1997). To verify that PDGFRα/PDGFRβ protein is eliminated, we used timed-pregnancies to obtain $aR^{\Delta Flp/\Delta Flp}$ embryos at E11.5 and $bR^{\Delta Flp/\Delta Flp}$ fetuses at E17.5. Tissue lysates showed complete absence of PDGFRα or PDGFRβ in the respective homozygotes compared to heterozygotes (Supplementary Fig. 2g,h). PDGFRα was hyperphosphorylated in $aR^{\Delta K.Flp/+}$*;Sox2-Cre* embryos at E13.5 (Supplementary Fig. 2f,i). Cre-dependence was also shown *in vitro* by transduction of Cre-expressing virus or control virus into dermal fibroblasts from $aR^{Flp/Flp}$, $bR^{Flp/Flp}$, or $aR^{\Delta K.Flp/+}$ mice, followed by Western blotting (Fig. 1b-d).

Lineage Labeling with Pdgfr-Flp Knockin Mice

The $aR^{\Delta Flp/+}$ and $bR^{\Delta Flp/+}$ mice provided an opportunity to trace the fates of embryonic $PDGFR\alpha^+$ and $PDGFR\beta^+$ cells by crossing with the *R26-frt.Stop.frt-tdTomato* reporter (denoted as *fSf-Tomato*). We verified that Cre-naïve $aR^{Flp/Flp}$, $bR^{Flp/Flp}$, and $aR^{K.Flp/+}$ mice could not activate *fSf-Tomato* (Supplementary Fig. 3a-c). However, in $aR^{\Delta Flp/+}$ *Sox2-Cre*^{tg}

mice with *fSf-Tomato,* all detectable subcutaneous and visceral WAs and interscapular BAs were Tomato$^+$ (Fig. 1e). This is consistent with a previous study that used *Pdgfra-Cre^{tg}* transgenic mice (Berry and Rodeheffer, 2013). We also found that *bR$^{\Delta Flp/+}$Sox2-Cre^{tg}* mice with *fSf-Tomato* achieved partial Tomato-labeling of WAs and BAs at P21 (Fig. 1f), consistent with previous studies using *Pdgfrb-Cre^{tg}* transgenic mice (Tang et al., 2008).

Adipocyte progenitors (APs) reside locally in the stromal-vascular fraction (SVF) of adipose tissue, which also includes immune cells, endothelial cells, and non-adipogenic fibroblasts. APs can be identified by flow cytometry based on the expression of mesenchymal and progenitor cell markers (CD29 and CD34), while negative for erythroid, lymphoid, and endothelial cell markers (Ter119, CD45, and CD31) (Supplementary Fig. 4). In white adipose tissue (WAT) from P21 *aR$^{\Delta Flp/+}$* mice and *bR$^{\Delta Flp/+}$* mice, Tomato$^+$ cells were 35-40% of the total live cellular SVF and 84-95%% of APs (Fig. 1g,h). Therefore, the embryonic *Pdgfra*- and *Pdgfrb*-lineages here label portions of the total SVF, and both are enriched in APs, consistent with previous studies using transgenic mice (Berry and Rodeheffer, 2013; Gao et al., 2018; Tang et al., 2008).

Lastly, we created timed pregnancies between *aR$^{K.Flp/+}$;fSf-Tomato* mice and *Sox2-Cre^{tg}* mice to obtain *aR$^{\Delta K.Flp/+}$* embryos, which were viable at E13.5 with Tomato labeling of PDGFRα^K-expressing cells (Fig. 1i). Tomato was broadly expressed in mesenchymal cells of the frontonasal prominence but not in cells of the nasal epithelium, the olfactory lobe, or the overlying epidermis (Fig. 1j). Since viable *aR$^{\Delta K.Flp/+}$* embryos could not survive later than E13.5 and the earliest fat depots do not appear until E14.5 (Han et al., 2011; Schulz and Tseng, 2013), lineage tracing aR-ΔK.Flp mutant cells in adipose tissue requires an inducible system.

Different Adipogenic Properties of Mosaic PDGFRα$^+$ and PDGFRβ$^+$ Cells in Adult Mice

To examine adult PDGFRα$^+$ and PDGFRβ$^+$ cell labeling with an inducible system, we used *Ubc-CreER^{tg}* to globally express Tamoxifen (Tmx)-regulated Cre under control of the *Ubiquitin C* promoter. As there is no perfect Cre driver for APs, we chose *Ubc-CreER^{tg}* to be as inclusive as possible in our analysis, relying on the endogenous *Pdgfra*- and *Pdgfrb*-promoters to control Flp^o expression. Hence, we generated mice with *Ubc-CreER^{tg}* and *fSf-Tomato* plus heterozygosity for the Cre-naïve knockin cassette (i.e. *aR$^{Flp/+}$* or *bR$^{Flp/+}$*). After verifying Tomato expression only in the presence of *Ubc-CreER* and Tmx (Supplementary Fig. 3d-f), we administered a single dose of Tmx (100mg/kg) to 6-week-old mice and analyzed them one week later (Fig. 2a). This approach generated mosaic tissues where most cells remain Cre-naïve but a subset of cells convert to the *aR$^{\Delta Flp/+}$* or *bR$^{\Delta Flp/+}$* genotype, which allows them to become Tomato$^+$ if they are a cell type with a sufficiently active *Pdgfr* promoter to drive Flp^o expression.

By flow cytometry, Tomato was enriched in WAT-derived APs compared to total SVF from mosaic *Pdgfra* and *Pdgfrb* mice regardless of sex (Fig. 2b). We also assessed Cre/lox recombination at the genomic DNA level using quantitative PCR to measure deletion of the PDGFRα/PDGFRβ cDNAs. The average recombination rate was lower in mosaic *Pdgfra* compared to *Pdgfrb* (Fig. 2c), indicating that the *Pdgfra* locus is less accessible to Cre.

Importantly, the same PCR primers are used to detect PDGFRα or PDGFRβ cDNA deletion because of sequences common to both targeting vectors (Supplementary Fig. 1a,b).

Adipose tissues from mosaic mice were histologically indistinguishable from tissues of mice without Tmx (Supplementary Fig. 5a,b). By fluorescence microscopy, scattered Tomato$^+$ cells in mosaic *Pdgfra* WAT exhibited a fibroblast-like appearance and were co-stained with PDGFRα antibody that was validated on $aR^{\Delta Flp/\Delta Flp}$ tissue (Supplementary Fig. 5c,e). Also scattered throughout the tissue were Tomato$^+$ cells with a balloon-like morphology and attached nucleus, which were confirmed as adipocytes with Plin1 antibody staining (Fig. 2d). As PDGFRα is downregulated during adipogenesis and is not expressed in mature adipocytes, Tomato$^+$ adipocytes are derived from PDGFRα$^+$ APs. Labeled adipocytes occurred as single cells or as clusters, consistent with stochastic labeling of APs along a proliferation/differentiation trajectory (Burl et al., 2018). For quantification, we devised an adipocyte index as the number of Tomato$^+$ WA divided by the total number of Tomato$^+$ cells (WA + stromal cells). We generated this measurement in five different depots: inguinal WAT (ingWAT), perigonadal WAT (pWAT), anterior subcutaneous WAT (asWAT), retroperitoneal WAT (rWAT), and mesenteric WAT (mWAT). For reasons that remain unclear, there was variability in adipocyte index with some mice having more than 50% adipocytes among their Tomato$^+$ cells and others labeled only stromal cells (Fig. 2e). The average index ranged from 10% to 25% across different fat depots. Therefore, some PDGFRα$^+$ cells in adult WAT undergo adipogenesis within 7 days of Tmx, most likely reflecting variations in basal adipogenesis. We obtained similar results in BAT 1 week after Tmx, with many Tomato$^+$ BAs in mosaic *Pdgfra* BAT and high inter-animal variability (Fig. 2f).

Unlike *Pdgfra,* most Tomato$^+$ cells in adult mosaic *Pdgfrb* WAT were mural cells, either vascular smooth muscle cells (VSMCs) or pericytes (Fig. 2h) and were co-stained with PDGFRβ antibody that was validated on $bR^{\Delta Flp/\Delta Flp}$ tissue (Supplementary Fig. 5d,f). However, Tomato$^+$ adipocytes were not observed in any WAT at 7 days after Tmx (Fig. 2i). The result was similar in mosaic *Pdgfrb* BAT (Fig. 2j,k). Therefore, the adult population labeled in mosaic *Pdgfrb* fat consists mainly of mural cells that do not differentiate into adipocytes within 7 days of Tmx.

Expression of PDGFRα and PDGFRβ in the vascular adventitia

Intriguingly, we occasionally saw single Tomato$^+$ cells in adult mosaic *Pdgfrb* WAT that were positioned in the perivascular adventitia outside the VSMC layer. We suspected that these cells might be inefficiently labeled in the mosaic setting. To address this we administered 100mg/kg Tmx for 5 days and then analyzed after 7 more days (Fig. 3a). Although higher Tmx still did not generate Tomato$^+$ adipocytes, it did produce robust labeling of adventitial fibroblasts (Fig. 3b). Moreover, when mosaic *Pdgfra* mice were administered high Tmx there was a strikingly similar pattern of labeled adventitial fibroblasts (Fig. 3a,c). To investigate potential co-expression of *Pdgfra/Pdgfrb*-reporters, we crossed $bRFlp^{Flp/+}$ mice (genotype $Pdgfrb^{Flp/+}$;*Ubc-CreER*^{tg};*fSf-Tomato*) with $Pdgfra^{H2BEGFP/+}$ knockin mice to create a double reporter (Fig. 3d). Here, PDGFRα$^+$ cells are continually marked with a nuclear-localized EGFP, and cells with current or prior *Pdgfrb* expression are mosaically labeled with Tomato. Note that H2B-EGFP is a stable protein and

dim expression was detectable in some adipocyte nuclei (Supplemental Fig. 6a), consistent with PDGFRα expression in APs prior to terminal differentiation (Lee et al., 2012). At one week after 1x Tmx, most Tomato$^+$ cells were mural cells wrapped around CD31$^+$ capillaries and arterioles, and EGFP$^+$ nuclei could be distant from vessels or juxtaposed to vessels but nearly always distinct from Tomato$^+$ cells (Fig. 3e), indicating that mosaic bR-Flp/Tomato and constitutive aR-H2BEGFP reporters are largely non-overlapping. Nevertheless, when we used confocal microscopy to create z-stacks of adipose tissue vasculature, instances of co-expression (red cytoplasm/yellow nucleus) were seen when Tomato labeling occurred in adventitial fibroblasts (Fig. 3f)(Supplementary Videos 1-3).

A doxycycline inducible *Pdgfrb-rtTA;TRE-Cre* system can lineage trace a significant portion of WAs in pWAT after 8 weeks, and this labeling can be further increased by feeding HFD (Vishvanath et al., 2016). It is currently controversial whether this labeling reflects PDGFRβ$^+$ mural cells or adventitial fibroblasts as a long-term source of WAs (Guimaraes-Camboa and Evans, 2017). To further investigate this question with our model, we generated mosaic *Pdgfrb* mice with 1x Tmx and then fed HFD for 8 weeks, but we could only detect rare Tomato$^+$ WAs comprising <1% of the Tomato$^+$ cell population in any tissue (Supplementary Fig. 6b,c). Next we generated *Pdgfrb* mice with 5x Tmx for adventitial fibroblast labeling and fed normal chow or HFD for 8 weeks (Fig. 3g). HFD caused obesity with a significant increase in % body fat and WAT expansion (Supplemental Fig. 6e-g). There was strong Tomato labeling of adventitial fibroblasts and many WAs independent of diet (Fig. 3h,i). Furthermore, in mice that were fed HFD, the adipocyte index was significantly increased in pWAT and rWAT, two visceral depots susceptible to HFD-induced hyperplasia (Fig. 3j)(Shao et al., 2018). Tomato$^+$ BAs were also detected in BAT with widespread labeling, but HFD did not increase the index (Supplemental Fig. 6h). Therefore, adult PDGFRβ$^+$ cells can give rise to new adipocytes with time, and this lineage tracing requires widespread (non-mosaic) labeling conditions that efficiently target adventitial fibroblasts. Taken together, these data suggest an adult adipogenic niche composed of CD31$^+$ blood endothelial cells, PDGFRβ$^+$ mural cells, and adventitial APs expressing both PDGFRα/PDGFRβ.

Inactivation of PDGFRα or PDGFRβ in Postnatal Progenitors Enhances Adipogenesis

Next we turned to the question of whether the PDGFRs have a functional role in adipogenesis is not known. To investigate PDGFRα, we designed experiments to produce mosaic knockout mice by pairing a conditional Flp allele with a null allele (e.g. $aR^{Flp/-}$) so that *Ubc-CreER*^{tg} induces Tomato$^+$ cells with no PDGFRα (e.g. $aR^{\Delta Flp/-}$). Mosaic control mice have a conditional Flp allele paired with a wild-type allele (e.g. $aR^{Flp/+}$), which Cre converts to Tomato$^+$ cells that retain PDGFRα (e.g. $aR^{\Delta Flp/+}$) (Supplementary Fig. 7). We gave a single Tmx dose of 50mg/kg to pregnant females to induce recombination in the fetus at E18.5 when WAT is still immature, for analysis at P7 or P21 (Fig. 4a). At P7, Tomato$^+$ cells were only 0.1% of the total SVF in WAT, but they were highly enriched in the AP population (Fig. 4b). Mosaicism was similar between genotypes at the gDNA level (Fig. 4c). *Pdgfra* control and knockout mice grew normally and there was no histological difference in WAT/BAT at P21. In both genotypes there were abundant Tomato$^+$ stromal cells and WAs (Fig. 4d). As shown in Fig. 4e, the adipocyte index was increased in knockout WAT compared to control. Most of the Tomato$^+$ cells in control BAT were brown adipocytes with

only a minor population of stromal cells (Fig. 4f). There was an increase in Tomato$^+$ BAs in knockout BAT compared to control (Fig. 4g). Therefore, PDGFRα is not required for adipocyte differentiation, but instead removal of PDGFRα increases differentiation.

Using the same approach for PDGFRβ (Fig. 5a, Supplementary Fig. 7), Tomato labeling in P7 WAT from *Pdgfrb* control and knockout was 0.5% or less of the total SVF and was enriched in the AP population (Fig. 5b). There was lower gDNA mosaicism in knockouts (Fig. 5c). Both genotypes grew normally with no histological difference in WAT/BAT at P21. Differences were immediately apparent in Tomato$^+$ cell labeling, however, with a striking reduction in Tomato$^+$ mural cells in the knockout (Fig. 5d,e). This was expected because PDGFRβ is required for proliferation and maintenance of VSMCs and pericytes (Crosby et al., 1998; Lindahl et al., 1997). Since Tomato$^+$ cells in knockout mice lack PDGFRβ (genotype: $bR^{\Delta Flp/-}$), they are at a competitive disadvantage compared to cells in their milieu that retain PDGFRβ. Adipocytes were also labeled in control and knockout mice lineage traced from E18.5 to P21 (Fig. 5f), and in contrast to the mural cell compartment where PDGFRβ deletion leads to fewer Tomato$^+$ mural cells, there was a dramatic increase in Tomato$^+$ WAs in knockout WATs (Fig. 5g,h), Therefore, PDGFRβ is not required for postnatal adipogenesis, but instead, inactivation of PDGFRβ facilitates WA differentiation. There were also many Tomato$^+$ BAs in both *Pdgfrb* genotypes at P21 (Fig. 5i), and the index was increased in knockouts (Fig. 5j). From these data we conclude that both receptors oppose adipogenesis, potentially by controlling downstream signaling pathways that inhibit progression towards differentiation.

PDGFRα^K Inhibits Differentiation but Progenitors Retain Adipogenic Potential

Elevated PDGFRα signaling causes APs to become myofibroblast-like cells that secrete excess ECM (Iwayama et al., 2015). Although this causes WAT lipoatrophy (Sun et al., 2017), it is unclear whether PDGFRα signaling directly inhibits adipogenesis from APs *in vivo*. To investigate adipogenesis in the absence of overt tissue fibrosis, we crossed *Ubc-CreER^{tg}* mice with Cre-naïve $aR^{K.Flp/+}$;*fSf-Tomato* mice and administered Tmx at E18.5 to obtain mosaic PDGFRα^K mice (Fig. 6a,c). Tmx dosage was reduced to 10mg/kg to avoid fibrosis. Tomato labeling in the overall SVF was only 0.4%, but almost 4% of the APs were labeled (Fig. 6b). At P21, $aR^{K.Flp/+}$ WAT was indistinguishable from Tmx-treated wild-type mice, with no evidence of fibrosis (Fig. 6d). These mice were nearly devoid of Tomato$^+$ WAs, strongly suggest that PDGFRα^K signaling inhibits adipogenesis directly and cell-autonomously. However, Tomato$^+$ WAs began to emerge by 4-6 weeks of age, albeit at a rate far lower than mosaic *Pdgfra* control WAT (compare y-axis of Fig. 4e and Fig. 6e). Tomato$^+$ BAs were <10% of the total Tomato$^+$ cells in $aR^{K.Flp/+}$ BAT at P21, again in contrast with the high adipocyte index in mosaic *Pdgfra* control BAT (compare Fig. 4g and Fig. 6f). Together, these results strongly suggest that PDGFRα^K signaling inhibits adipogenesis directly and cell-autonomously, but not permanently. To further investigate the reversibility of PDGFRα^K effects, we used a PDGFR-selective kinase inhibitor, Crenolanib (Heinrich et al., 2012). We generated mosaic $aR^{K.Flp/+}$ mice with Tmx at E18.5 and administered Crenolanib or vehicle from P21 until P28 (Fig. 6g). Crenolanib significantly increased adipogenesis compared with vehicle-treated counterparts (Fig. 6h,i), further supporting the conclusion that PDGFRα^K does not erase adipogenic potential.

Inactivation of PDGFRα/PDGFRβ Enhances Adrb3-induced Beige Adipogenesis

Beige adipocytes (bAs) have functional similarities to BAs in generating heat but they are induced in WAT in response to cold temperature or stimulation with β3-adrenergic receptor (Adrb3) agonists (Ikeda et al., 2018). The Adrb3 agonist CL316,243 (CL) can induce *de novo* beige adipogenesis from PDGFRα^{+} progenitors specifically in pWAT (Lee et al., 2013; Lee et al., 2012). It has been suggested in cell lines that PDGFRα promotes bA differentiation and PDGFRβ counteracts it (Gao et al., 2018). If this operates *in vivo* and occurs cell-autonomously, then mosaic *Pdgfra* knockout should impair bA differentiation and mosaic expression of PDGFRα^{K} or *Pdgfrb* knockout might enhance it. We generated a cohort including each of the five adult mosaic lines described in this study: $aR^{Flp/+}$ controls, $aR^{Flp/Flp}$ knockouts, $aR^{K.Flp/+}$ mice with elevated PDGFRα signaling, $bR^{Flp/+}$ controls, and $bR^{Flp/-}$ knockouts. Tmx was administered at 6 weeks of age and then after 1 week of recovery we injected CL for 11 days (Fig. 7a). Here we used $aR^{Flp/Flp}$ mice instead of $aR^{Flp/-}$ mice because we noticed that by 6 weeks old some $aR^{Flp/-}$ mice exhibited runting and poor survival irrespective of Tmx treatment, suggestive of an age-dependent hypomorphic phenotype in $aR^{Flp/-}$ mice. Histological analysis confirmed pWAT beiging in all Tmx/CL-treated mice (Fig. 7b). Tomato^{+} bAs were most frequently seen in $aR^{Flp/Flp}$ knockouts, followed by $aR^{Flp/+}$ controls (Fig. 7c). $aR^{K.Flp/+}$ mice and $bR^{Flp/+}$ controls exhibited near-zero bA labeling. A small number of Tomato^{+} bAs were seen in $bR^{Flp/-}$ knockouts (Fig. 7c). There were also Tomato^{+} WAs in $aR^{Flp/+}$ and $aR^{Flp/Flp}$ mice (not shown), consistent with basal white adipogenesis in the week between Tmx and the initiation of CL. We calculated an index for bAs by dividing the number of Tomato^{+} bAs by the total number of Tomato^{+} cells counted (bA + WA + stromal cells). $aR^{Flp/Flp}$ and $bR^{Flp/-}$ knockouts showed a significantly higher bA index compared with their respective $aR^{Flp/+}$ and $bR^{Flp/+}$ controls (Fig. 7d). Some Tomato^{+} multilocular cells that we scored as bAs were Ucp1^{+}, but most were negative (Fig. 7e), consistent with the finding that many bAs in pWAT are indeed Ucp1 negative (Bertholet et al., 2017). In conclusion, the reciprocal increase in bA labeling with mosaic *Pdgfra* knockout and absence of labeling with PDGFRα^{K} shows that PDGFRα directly opposes CL-induced beige adipogenesis. And although adult PDGFRβ^{+} cells do not contribute to *de novo* bAs under these conditions, mosaic *Pdgfrb* knockout allows some lineage contribution to bAs. Therefore, PDGFRα or PDGFRβ downregulation facilitates lineage contribution to CL-induced beige adipogenesis.

DISCUSSION

In this study we show that the progenitor cell markers PDGFRα and PDGFRβ function as gatekeepers of adipocyte differentiation and their depletion facilitates adipogenesis in functional genetic mosaics *in vivo*. Conversely, constitutive activation of PDGFRα cell-autonomously blocks adipogenesis in the absence of fibrosis, and this block is reversible. Our major finding applies to postnatal development of WAs and BAs, and bA differentiation induced by Adrb3 activation in adult mice. These results imply that downregulation of PDGF signaling regulates the transition from progenitor to mature adipocyte.

The elucidation of gene function *in vivo* depends on identifying direct, cell-autonomous consequences of gene manipulation. This is sometimes difficult because mutations that

affect entire lineages can trigger homeostatic mechanisms that mask the direct effects. As a relevant example, conditional *Pdgfrb* knockout in adult mice, either globally or in PPARγ^{+} adipocyte progenitors, has significant physiological consequences, including deleterious effects on the vasculature and reduced adipose tissue mass, but with an overall improvement in glucose tolerance (Jiang et al., 2017; Onogi et al., 2017). But whether *Pdgfrb* perturbations directly affect adipocyte differentiation *in vivo* cannot be elucidated from such a complex phenotype. Similarly, constitutive PDGFRα^{K} signaling caused progressive adipose tissue fibrosis, but it was unclear whether the *in vivo* effects on adipocytes were direct or secondary to fibrosis (Iwayama et al., 2015). We adopted a functional genetic mosaic approach to more precisely define *Pdgfra/Pdgfrb* gene function. The genetic mosaic approach creates a few mutant cells while leaving most cells as non-mutant. Consequently, non-mutant cells provide a normal environment to protect against secondary effects on organ function. Non-mutant cells can also alleviate homeostatic mechanisms that mask weaker phenotypes. Mosaic analysis has been performed for many genes in the Drosophila genome (Xu and Rubin, 2012), and several different approaches have been explored in mammalian models (Lao et al., 2012; Pontes-Quero et al., 2017; Zong et al., 2005).

The three knockin constructs described in this study uniquely combine Cre/lox-mutagenesis of the endogenous *Pdgfra/Pdgfrb* genes with expression of Flp^{o} recombinase, which can be used to lineage label mutant cells. Flp^{o} expression is dependent on the endogenous *Pdgfr* promoter, and needs to be expressed at a sufficiently high level to induce recombination of its reporter target. Our experimental design generates Cre recombination in some cell types that do not become labeled because they are negative or low for *Pdgfr* expression. Therefore, while all labeled cells are mutant, the label is expected to underestimate the overall prevalence of mutant cells. The use of *Ubc-CreER^{tg}* was intended to maximize the diversity of the founder cell population, capturing any cells with a sufficiently active *Pdgfr* promoter at the time of Cre/loxP recombination, plus any cells that acquire *Pdgfr* promoter activity during the experiment. A final technical point relates to cell labeling with these constructs in heterozygous cells, which have reduced *Pdgfr* expression by 50% compared to neighboring cells. It is possible that the relative difference in *Pdgfr* expression could influence the behavior of labeled control cells. The potential for allele reduction to influence cell behavior is a consideration for any knockin/knockout model.

A portion of this work focused on lineage labeling to characterize adipogenic potential. We found that nearly all APs develop from an embryonic *Pdgfra*-lineage, while the *Pdgfrb*-lineage shows partial labeling in development. Because we used *Sox2-Cre^{tg}* to target the epiblast, we interpret this labeling to reflect maximal contribution from each lineage, and our results are consistent with previous studies using Pdgfr-Cre transgenes (Berry and Rodeheffer, 2013; Tang et al., 2008). In adult mice, we found that *Pdgfra*-lineage cells became adipocytes within 7 days of Tmx in all tissues examined. We interpret this as reflecting continual basal adipogenesis because we used low Tmx to minimize drug-induced adipocyte turnover (Ye et al., 2015). We found that the frequency of *Pdgfra*-lineage AP differentiation was highly variable between animals, with some having more than 50% adipocytes in Tomato^{+} cells and others displaying almost exclusively stromal cells. Further studies are needed to elucidate variables that influence basal adipogenesis, as indirect measurements have similarly shown that adipocyte hyperplasia is highly variable between

individual humans (Arner et al., 2010). In contrast, mosaic *Pdgfrb*-lineage cells in adult mice did not become adipocytes within 7 days of Tmx. Further exploration of *Pdgfrb*-lineage cells under non-mosaic conditions revealed labeling of adventitial cells on medium and large-sized blood vessels. These cells are distinct from VSMCs and reside in a separate layer surrounding the vascular media. Again, adipocytes were not labeled by the *Pdgfrb*-lineage within 7 days of high Tmx treatment. However, when these mice were aged for 8 weeks, we could find lineage contribution to adipocytes. Adipogenesis was significantly increased in visceral fat with HFD feeding. This finding of long-term adipogenesis from the *Pdgfrb*-lineage is congruent with lineage tracing with *Pdgfrb-rtTA;TRE-Cre* mice (Vishvanath et al., 2016), but since we could only label adipocytes under conditions where adventitial fibroblasts were also highly labeled, our result suggests that PDGFRβ$^+$ APs are adventitial fibroblasts, not mural cells. Moreover, we found that non-mosaic conditions generated adventitial cell labeling from the *Pdgfra*-lineage. Co-labeling of adventitial fibroblasts with constitutive *Pdgfra-H2BGFP* and mosaic *Pdgfrb*-lineage together suggest that double-positive adventitial fibroblasts are long-term APs. Our results are consistent with recent studies where mural cell derived adipogenesis was carefully examined using *Tbx18^{CreER}* for lineage tracing. Unlike PDGFRα$^+$ cells, Tbx18$^+$ mural cells scarcely differentiated into adipocytes (Cattaneo et al., 2020; Guimaraes-Camboa et al., 2017). Together with our findings, these independent results demonstrate that adventitial fibroblasts are the primary PDGFRβ$^+$ cell type that contributes to adipogenesis rather than PDGFRβ$^+$ mural cells.

Constitutive PDGFRα signaling generates fibrosis by causing APs to become matrix secreting myofibroblast-like cells (Iwayama et al., 2015), but it was unknown whether the opposite could be true: that reduced signaling could enhance adipogenesis. Here we show that mosaic deletion of *Pdgfra* or *Pdgfrb* significantly increased the proportion of Tomato$^+$ cells that differentiated into WAs or BAs *in vivo*. This regulatory effect was not limited to postnatal adipogenesis but also affected bA formation in adulthood. Together, these findings suggest that extinguishing PDGFRα or PDGFRβ signaling is an important regulated event necessary for adipocyte differentiation. Future studies may focus on the events that lead to PDGFR downregulation, and which PDGFR signaling pathways oppose adipogenesis. Increasing the overall number of white and brown/beige adipocytes is predicted to confer health benefits by increasing lipid storing capacity and energy expenditure (Kajimura et al., 2015; Kim et al., 2007; Wang et al., 2013). Promoting adipogenesis through PDGFR inhibition could also allow tissues to escape from fibrosis by channeling myofibroblasts into adipocytes. Therefore, knowledge about the mechanisms that regulate adipocyte populations in the body might be manipulated for therapeutic purposes (Cawthorn et al., 2012; Kusminski et al., 2016).

STAR METHODS

LEAD CONTACT AND MATERIALS AVAILABILITY

Further information and requests for resources and reagents should be directed to the Lead Contact, Lorin E. Olson (Lorin-Olson@omrf.org). Unique mice generated in this study are available from the Lead Contact with a completed Materials Transfer Agreement.

EXPERIMENTAL MODEL AND SUBJECT DETAILS

Mice—All animal experiments were performed according to procedures approved by the Institutional Animal Care and Use Committee at the Oklahoma Medical Research Foundation. Mice were maintained in a 12 hr light/dark cycle and housed in groups of two to five with unlimited access to water and food. All strains were maintained on a mixed C57BL/129 genetic background at room temperature. The lines *Sox-2Cre*^{tg} (JAX:008454) (Hayashi et al., 2002) and *Ubc-CreER*^{tg} (JAX:007001)(Ruzankina et al., 2007) were purchased from the Jackson Laboratories. *PDGFRa*$^{H2B:EGFP}$ (JAX:007669)(Hamilton et al., 2003) was a gift from Dr. Philippe Soriano. The line *Rosa26*$^{LSL\text{-}fSf\text{-}tdTomato}$ (JAX:021875) (Madisen et al., 2015) was purchased from the Jackson Laboratories and crossed with *Sox2-Cre*^{tg} to eliminate the *loxP*-flanked stop cassette, rendering it a Flp/frt-regulated reporter. The lines *Pdgfra*^{floxed} and *Pdgfrb*^{floxed} (JAX:006492, 010977)(Schmahl et al., 2008; Tallquist et al., 2003) were gifts from Philippe Soriano and were crossed with *Sox2-Cre*^{tg} to generate null alleles. Following these genetic modifications, *Sox2-Cre*^{tg} was eliminated by breeding, and the resulting *Rosa26*$^{fSf\text{-}tdTomato}$, *Pdgfra*$^{+/-}$, and *Pdgfrb*$^{+/-}$ mice were used for our studies.

The aR-Flp, aR-K.Flp and bR-Flp cassettes were knocked into the endogenous *Pdgfra* or *Pdgfrb* loci by homologous recombination in ES cells. The aR-Flp targeting vector (Figure S1A) was designed to insert a SA.lox.PDGFRα.lox-Flp^{o}-attB-Neo-attP cassette into the endogenous *Pdgfra* gene. We modified the previous targeting vector (Olson and Soriano, 2009) by replacing the lox-Neo/Stop-lox cassette with a lox-PDGFRα-lox cassette, and the PDGFRα^{K} cDNA was replaced with Flp^{o} cDNA. Furthermore, a new neomycin-resistance cassette was inserted downstream of Flp^{o} with flanking attB/attP sequences to allow removal of the resistance cassette by PhiC31. The aR-K.Flp targeting vector (Figure S1C) was designed to insert a SA.lox.Neo/Stop.lox-PDGFRα^{K}.T2A.Flp cassette in place of exons 2-4 of the endogenous *Pdgfra* gene. Thus, aR-K.Flp was based on a previously described vector (Olson and Soriano, 2009) with modification to replace the PDGFRα^{K} stop codon with nucleotides encoding a self-cleaving T2A sequence and a codon-optimized Flp^{o} recombinase (Kranz et al., 2010; Raymond and Soriano, 2007). The PDGFRα^{K} protein has a point mutation, D842V, which renders it constitutively active. The bR-Flp targeting vector (Figure S1B) was designed to insert a SA.lox.PDGFRβ.lox-Flp^{o}-attB-Neo-attP cassette in place of exons 2-4 the endogenous *Pdgfrb* gene. Thus, bR-Flp was based on a pervious vector (Olson and Soriano, 2011) with modification to replace the lox-Neo/Stop-lox cassette with a lox.PDGFRβ.lox cassette, and the PDGFRβ cDNA was replaced with Flp^{o} cDNA. A neomycin-resistance cassette was inserted downstream of Flp^{o} with flanking attB/attP sequences. Correctly targeted ES cells were identified by PCR and confirmed by Southern blotting as previously described (Olson and Soriano, 2009, 2011). The attB-Neo-attP cassettes were removed from ES cells by transiently expressing codon-optimized PhiC31^{o} (Raymond and Soriano, 2007). Chimeric males were generated by standard blastocyst injection and transplantation procedures. For aR-Flp and aR-K.Flp, PCR genotyping of genomic DNA was performed using three primers, aex2, ain2, and aex3, which generates a 306bp band for wild type *Pdgfra* and a 166bp band for either knockin. For bR-Flp, PCR genotyping was performed with three primers, bex2, bin2, and bex3, which generates a 346bp band for wild type *Pdgfrb* and a 160bp band for the knockin.

Tmx (Sigma T5648) was prepared as a 20mg/ml stock in corn oil. For mosaic Cre-recombination at 6 weeks old, mice were ip injected or gavaged with 100mg Tmx/kg bw, except for mosaic PDGFRα^{K} mice, which received only 10mg/kg. Mosaic mice were fed normal chow diet (Purina 5053) or high fat diet (Research Diets D12492), as indicated in the text. For non-mosaic Cre-recombination, 8 week old mice were gavaged with 100 mg Tmx/kg bw for 5 consecutive days. For mosaic Cre-recombination in the fetus, pregnant dams were gavaged with 50 mg Tmx/kg body weight (bw) at E18.5. The resulting offspring were analyzed at P7 or P21. For Crenolanib treatments (Selleck S2730), P21 mosaic PDGFRα^{K} mice mice were randomly allocated into drug or vehicle groups, which were ip injected daily with 15mg Crenolanib/kg bw or vehicle for 7 days. Crenolanib was prepared as a 50 mg/ml stock, which was diluted in glycerol formal (vehicle) to 1 mg/ml. For CL316,243 (CL) treatments (Cayman 17499), mice were injected with 100mg Tam/kg bw, followed by 1-week wash out period, followed by ip injection of 1 mg CL/kg bw for 11 days. Both males and females were analyzed.

METHOD DETAILS

Viral Transduction of Dermal Fibroblasts—Lentiviral constructs were created to constitutively express Cre-IRES-iRFP720 or IRES-iRFP720 (no Cre) from the hybrid promoter mCMV/EF1alpha/HTLV (InVivoGen), which is highly active in mouse cells. Generation of lentiviral particles and transductions were performed as previously described (Berry et al., 2014). Following transductions, dermal fibroblasts were cultured in DMEM + 10% FBS, 2mM L-glutamine, and 2mM pen/strep were selected with 1μg/mL puromycin, and then subjected to Western blot as described below.

Western Blotting—Protein was extracted from embryonic/fetal tissue or adult lung by mincing tissue in 1ml ice cold RIPA buffer (50mM Tris pH7.4, 150mM NaCl, 1% NP-40, 0.1% SDS, 0.25% sodium deoxycholate) with the addition of protease and phosphatase inhibitors (Complete protease inhibitor cocktail (Sigma 11836170001), 1mM EDTA, 1mM sodium orthovanadate, 1mM NaF, 1mM PMSF). After 10 minutes incubation on ice, lysates were sonicated for 30 seconds, followed by incubation on ice for one hour. The lysate was cleared by centrifugation. Protein concentration was determined by BCA assay (Pierce 23225). Similar procedures were used to isolate protein from viral transduced cells. For Western blotting, equal amounts of each protein sample (40 μg from embryo or 75 μg from lung) were separated by 8% gel SDS-PAGE, using two gels run in parallel. Proteins were transferred from gel to nitrocellulose membranes, blocked with 5% BSA, and then subjected to Western blotting with antibodies against total PDGFRα (Santa Cruz 338), total PDGFRβ (Santa Cruz 432), or phospho-PDGFRα (Cell Signaling 24188). Membranes were then probed with horseradish-peroxidase conjugated anti-rabbit secondary antibody (Jackson 711-035-152) diluted in 5% milk. Primary and secondary antibodies were used at 1:2000 and 1:5000, respectively. Blots were developed with ECL Western blotting substrate (Pierce 32106) and autoradiography film.

Measurement of Recombination Efficiency by qPCR—gDNA was extracted from embryos, from pup ear punches, or from intestine sampled from necropsied adults. Minced tissue was incubated overnight at 55^{o}C in tissue digestion buffer (100mM Tris pH 7.4,

100mM NaCl, 25mM EDTA, 0.5% SDS, 200 micrograms/ml proteinase K). DNA was then extracted with phenol/chloroform, precipitated with 0.5 volumes 7.5M ammonium acetate and 3 volumes 100% ethanol, washed with 70% ethanol, and resuspended in 0.1X TE buffer (1mM Tris pH7.4, 0.1mM EDTA). Quantitative PCR was performed in duplicate using 50-100ng gDNA on a Bio-Rad iCycler with iTaq SYBR Green Supermix (Bio-Rad 1725122). To measure recombination efficiency, which is the % conversion of aR-Flp into aR-ΔFlp, and bR-Flp into bR-ΔFlp, primers SAF and FlpR were used to amplify the junction of the splice acceptor and the Flpo cDNA, which is created by deletion of the *lox-Pdgfra-lox* or *lox-Pdgfrb-lox* cassettes (Figure S1A, S1B). To measure the recombination of aR-K.Flp into aR-ΔKFlp, primers SAF and aRR were used to amplify the junction of the splice acceptor and PDGFRa^{K} cDNA, which is created by deletion of the *lox-Stop-lox* cassette (Figure S1C). In all cases, normalization was achieved with primers Flp1 and Flp2, which amplify the Flp^{o} cDNA. PCR efficiency was determined by comparison to a standard curve of gDNA from *aR$^{\Delta K.Flp/+}$;Sox2-Cre, aR$^{\Delta Flp/+}$;Sox2-Cre,* or *bR$^{\Delta Flp/+}$;Sox2-Cre* embryos.

Flow Cytometry—Adipose tissue was excised, minced with scissors, and digested in Hank's Balanced Salt Solution (HBSS) containing 0.3 mg/ml collagenase Type I, 3% BSA, 1.2 mM $CaCl_2$ and 1 mM $MgCl_2$ for 75 min with shaking at 37 °C. The suspension was filtered with 40 μm cell strainer and centrifuged at 500 g. Supernatant and the floating layer including adipocytes were removed and then the pellet was washed with FACS buffer (PBS with 2% FBS and 1mM EDTA). The pellet was stained with AF700 anti-mouse CD29 (1:100)(#102218), APC anti-mouse CD34 (1:20)(# 119310), BV421 anti-mouse CD45.2 (1:40)(#109831), PerCP/Cy5.5 anti-mouse CD31 (1:20)(# 102420), PE/Cy7 anti-mouse TER-119 (1:100)(#116221) and Zombie Green (1:1000)(#423111) (all from BioLegend). The staining was performed on ice for 10 min and then washed with FACS buffer. Stained samples were analyzed on a BD LSRII and data analysis was performed utilizing BD FACS Diva and FlowJo. Cells isolated from adipose tissue of Tomato-negative mice, along with primary-minus-one antibody combinations, and Tomato-positive mice, along with all antibodies, were used as the negative controls to determine the gates (see Supplementary Fig. 4).

Immunofluorescence Staining—Embryos were fixed in 4% paraformaldehyde for 16 h. After cryo embedding and sectioning (10-14 μm), sections were washed in PBS for 5 min and then incubated in PBS containing DAPI for 5 min. Samples were mounted with Fluoro Gel with DABCO (Electron Microscopy Sciences 17985-02). Adipose tissue was excised and fixed in 4% paraformaldehyde for 16 h. After paraffin embedding and sectioning (8 μm), sections were deparaffinized and rehydrated. For PDGFRα staining, antigen retrieval was performed by incubating in 10mM sodium citrate buffer pH6.0 with 0.05% Tween 20 for 30 min at 95-100 °C. All sections were blocked with 5% donkey serum for 1h at room temperature and incubated with primary antibodies for 24 h at 4 °C. The following primary antibodies were diluted in PBS containing 5% donkey serum and used: goat anti-Plin1 (1:300)(Novus 100-60554), rabbit anti-RFP (1:100)(Rockland 600-401-379), rabbit anti-UCP1 (1:100)(Abcam 10983) and goat anti-PDGFRα (1:250)(R&D AF1062). After washing in PBS, sections were incubated with secondary antibodies for 1 h at room temperature. The following secondary antibodies were diluted in PBS containing 5% donkey

serum and used: donkey anti-goat AF488 (1:100)(Jackson 705-545-003), donkey anti-rabbit Cy3 (1:100)(Jackson 711-545-003) and donkey anti-rabbit AF488 (1:100)(Jackson 711-545-152). After incubating in PBS containing DAPI, sections were mounted with Fluoro Gel with DABCO. For staining of PDGFRβ and αSMA, thick frozen sections (120 μm) were made. Sections were washed in PBS for 5 min and then incubated with primary antibodies for 24 h at 4 °C. The following primary antibodies were diluted in PBS containing 5% donkey serum and used: rat anti-PDGFRβ (1:200)(eBioscience 14-1402-82) and αSMA (1:200) (Cell signaling 19245). After incubating in PBS containing DAPI, sections were mounted with Fluoro Gel with DABCO. Sections were imaged by Nikon ECLIPSE 80i and analysed by Nikon NIS-Elements D3.2 or Nikon C2+ Confocal microscope and analysed by Nikon NIS-Elements AR. For wholemount staining, tissues were fixed in 4% paraformaldehyde/PBS overnight. Then samples approximately 2 mm^3 were washed in PBS and followed by x2 wash in PBS with 0.2% TritonX-100 for 1 hr. Samples were incubated in PBS with 0.2% TritonX-100 and 20% DMSO for 24 h and then incubated in PBS with 0.1% Tween-20, 0.1% TritonX-100, 0.1% NP40, 0.1% sodium deoxycholate and 20% DMSO for 24h. After x2 washes in PBS with 0.2% TritonX-100 for 1 hr, samples were incubated in PBS with 0.2% TritonX-100, 20% DMSO and 0.3M glycine for 24 h and followed by block in PBS with 0.2% TritonX-100, 10% DMSO and 6% serum for 24h. Samples were washed x2 in PBS with 0.2% Tween-20 and 10 μg/ml heparin (PTwH) for 1 hr and then incubated with rabbit anti-Plin1 (Cell Signaling 9349) or armenian hamster anti-CD31 (Abcam 10983) in PTwH with 5% DMSO and 3%serum for 48 hr. Samples were washed twice with PTwH for 1 hr and incubated with secondary antibodies (donkey anti-rabbit AF488 or goat anti-armenian hamster AF488 or donkey anti-rabbit AF647 or goat anti-armenian hamster AF647) diluted in PTwH with 3% donkey or goat serum for 24 hr. Then samples were washed in PTwH for 24 h and then mounted on a slide with mounting medium (Fluoro Gel with DABCO) and a barrier of Vaseline to seal the coverslip. All whole mount staining steps were performed at room temperature. Stained samples were imaged with a ZEISS LSM 710 confocal laser-scanning microscope and analysed by ZEISS ZEN microscope software.

Body Composition Analysis—Live mice were analyzed by EchoMRI Body Composition Analyzer (EchoMRI) and % body fat was calculated based on body weight. For tissue weight, one side of ingWAT or pWAT was weighed and divided by total body weight for % tissue weight.

QUANTIFICATION AND STATISTICAL ANALYSIS

Statistical Analysis—Data are presented as means + SD. Differences were analyzed by unpaired two-tailed Student's t test between two groups using Graphpad Prism 7. All measurements were from distinct biological samples. Statistical parameters are found in the figure legends, including exact n and number of biological repeats. Exact *P*-values are shown.

Quantification of Adipocyte Index for Tomato$^+$ Cells—Adipose tissue was fixed in 4% paraformaldehyde for 24 h and washed in PBS. Thin-sliced adipose tissue was mounted between a coverslip and slide. Scattered Tomato$^+$ WAs in mosaic whole mount WAT could

be distinguished from non-adipocytes by their distinct spherical morphology and attached nucleus, such that adipocyte marker co-staining was not routinely needed for manual quantification using a Nikon ECLIPSE 80i fluorescence microscope. A given WAT from an individual mouse was considered a biological replicate. Between 100 and 600 Tomato$^+$ cells were scored per WAT (depending on depot). For *Pdgfra* mosaics, all Tomato$^+$ cells were scored as adipocytes or stromal cells. For *Pdgfrb* mosaics, only adipocytes and pericytes were scored because it was difficult to unambiguously count single VSMCs. For each sample, the % Tomato$^+$ WAs was calculated by dividing the number of Tomato$^+$ WAs by the total number of Tomato$^+$ cells (WA + stromal cells). This index served to normalize for variable mosaicism from mouse to mouse. For BAT, and bAs in pWAT, paraffin tissue sections were used for quantification after staining with RFP/Tomato antibody. For BAT, the % Tomato$^+$ BAs was calculated by dividing the number of Tomato$^+$ BAs by the total number of Tomato$^+$ cells (BA + stromal cells). For bAs in pWAT, scattered bAs and WAs were distinguishable based on unambiguous multilocular or unilocular morphology, and the % Tomato$^+$ bAs was calculated by dividing the number of Tomato$^+$ bAs by the total number of Tomato$^+$ cells (bA + WA + stromal cells). Experiments were not blinded, as the mouse genotypes were known prior to analysis. Two independent investigators replicated the method of quantification (C.S. and H.S.).

DATA AND CODE AVAILABILITY

The quantitative datasets supporting the current study have been deposited in the “Mendeley Data” repository, dataset “Mosaic mutant analysis identifies PDGFRα/PDGFRβ as negative regulators of adipogenesis”, https://doi:10.17632/26r263sm6w.1.

Supplementary Material

Refer to Web version on PubMed Central for supplementary material.

ACKNOWLEDGEMENTS

We thank Linda Thompson, Sathish Srinivasan, Philippe Soriano, Juan Sanchez-Gurmaches, and members of the Olson lab for helpful discussions, and Kevin Kelley at the Icahn School of Medicine at Mt. Sinai Mouse Genetics and Gene targeting core for assistance in generating chimeric mice. We also thank the Flow Cytometry Core and Imaging Core Facilities (associated with P20-GM103636) and the Microscopy Core and Mouse Phenotyping Core Facilities (associated with P30-GM114731) of the Oklahoma Medical Research Foundation Centers of Biomedical Research Excellence. This study was supported by US National Institutes of Health (NIH) grants R01-AR070235 and P20-GM103636, and grants from the Oklahoma Center for Adult Stem Cell Research - a program of TSET (L.E.O). C.S. was supported by a predoctoral fellowship from the American Heart Association. L.E.O. is a Pew Scholar in Biomedical Research and this work was supported in part by the Pew Charitable Trusts.

REFERENCES

Andrae J, Gallini R, and Betsholtz C (2008). Role of platelet-derived growth factors in physiology and medicine. Genes Dev 22, 1276–1312. [PubMed: 18483217]

Armulik A, Genove G, and Betsholtz C (2011). Pericytes: developmental, physiological, and pathological perspectives, problems, and promises. Dev Cell 21, 193–215. [PubMed: 21839917]

Arner E, Westermark PO, Spalding KL, Britton T, Ryden M, Frisen J, Bernard S, and Arner P (2010). Adipocyte turnover: relevance to human adipose tissue morphology. Diabetes 59, 105–109. [PubMed: 19846802]

Berry R, and Rodeheffer MS (2013). Characterization of the adipocyte cellular lineage in vivo. Nat Cell Biol 15, 302–308. [PubMed: 23434825]

Berry WL, Kim TD, and Janknecht R (2014). Stimulation of beta-catenin and colon cancer cell growth by the KDM4B histone demethylase. International journal of oncology 44, 1341–1348. [PubMed: 24481461]

Bertholet AM, Kazak L, Chouchani ET, Bogaczynska MG, Paranjpe I, Wainwright GL, Betourne A, Kajimura S, Spiegelman BM, and Kirichok Y (2017). Mitochondrial Patch Clamp of Beige Adipocytes Reveals UCP1-Positive and UCP1-Negative Cells Both Exhibiting Futile Creatine Cycling. Cell Metab 25, 811–822 e814. [PubMed: 28380374]

Burl RB, Ramseyer VD, Rondini EA, Pique-Regi R, Lee YH, and Granneman JG (2018). Deconstructing Adipogenesis Induced by beta3-Adrenergic Receptor Activation with Single-Cell Expression Profiling. Cell Metab 28, 300–309 e304. [PubMed: 29937373]

Cattaneo P, Mukherjee D, Spinozzi S, Zhang L, Larcher V, Stallcup WB, Kataoka H, Chen J, Dimmeler S, Evans SM, et al. (2020). Parallel Lineage-Tracing Studies Establish Fibroblasts as the Prevailing In Vivo Adipocyte Progenitor. Cell reports 30, 571–582 e572. [PubMed: 31940497]

Cawthorn WP, Scheller EL, and MacDougald OA (2012). Adipose tissue stem cells: the great WAT hope. Trends in endocrinology and metabolism: TEM 23, 270–277. [PubMed: 22417866]

Crosby JR, Seifert RA, Soriano P, and Bowen-Pope DF (1998). Chimaeric analysis reveals role of Pdgf receptors in all muscle lineages. Nat Genet 18, 385–388. [PubMed: 9537425]

Gao Z, Daquinag AC, Su F, Snyder B, and Kolonin MG (2018). PDGFRalpha/PDGFRbeta signaling balance modulates progenitor cell differentiation into white and beige adipocytes. Development 145.

Guimaraes-Camboa N, Cattaneo P, Sun Y, Moore-Morris T, Gu Y, Dalton ND, Rockenstein E, Masliah E, Peterson KL, Stallcup WB, et al. (2017). Pericytes of Multiple Organs Do Not Behave as Mesenchymal Stem Cells In Vivo. Cell Stem Cell 20, 345–359 e345. [PubMed: 28111199]

Guimaraes-Camboa N, and Evans SM (2017). Are Perivascular Adipocyte Progenitors Mural Cells or Adventitial Fibroblasts? Cell Stem Cell 20, 587–589. [PubMed: 28475883]

Hamilton TG, Klinghoffer RA, Corrin PD, and Soriano P (2003). Evolutionary divergence of platelet-derived growth factor alpha receptor signaling mechanisms. Mol Cell Biol 23, 4013–4025. [PubMed: 12748302]

Han J, Lee JE, Jin J, Lim JS, Oh N, Kim K, Chang SI, Shibuya M, Kim H, and Koh GY (2011). The spatiotemporal development of adipose tissue. Development 138, 5027–5037. [PubMed: 22028034]

Hayashi S, Lewis P, Pevny L, and McMahon AP (2002). Efficient gene modulation in mouse epiblast using a Sox2Cre transgenic mouse strain. Mech Dev 119 Suppl 1, S97–S101. [PubMed: 14516668]

He C, Medley SC, Kim J, Sun C, Kwon HR, Sakashita H, Pincu Y, Yao L, Eppard D, Dai B, et al. (2017). STAT1 modulates tissue wasting or overgrowth downstream from PDGFRbeta. Genes Dev.

Heinrich MC, Corless CL, Duensing A, McGreevey L, Chen CJ, Joseph N, Singer S, Griffith DJ, Haley A, Town A, et al. (2003). PDGFrA activating mutations in gastrointestinal stromal tumors. Science 299, 708–710. [PubMed: 12522257]

Heinrich MC, Griffith D, McKinley A, Patterson J, Presnell A, Ramachandran A, and Debiec-Rychter M (2012). Crenolanib inhibits the drug-resistant PDGFRA D842V mutation associated with imatinib-resistant gastrointestinal stromal tumors. Clin Cancer Res 18, 4375–4384. [PubMed: 22745105]

Heldin CH, and Westermark B (1999). Mechanism of action and in vivo role of platelet-derived growth factor. Physiol Rev 79, 1283–1316. [PubMed: 10508235]

Hepler C, Shan B, Zhang Q, Henry GH, Shao M, Vishvanath L, Ghaben AL, Mobley AB, Strand D, Hon GC, et al. (2018). Identification of functionally distinct fibro-inflammatory and adipogenic stromal subpopulations in visceral adipose tissue of adult mice. eLife 7.

Hoch RV, and Soriano P (2003). Roles of PDGF in animal development. Development 130, 4769–4784. [PubMed: 12952899]

Hong KY, Bae H, Park I, Park DY, Kim KH, Kubota Y, Cho ES, Kim H, Adams RH, Yoo OJ, et al. (2015). Perilipin+ embryonic preadipocytes actively proliferate along growing vasculatures for adipose expansion. Development 142, 2623–2632. [PubMed: 26243869]

Ikeda K, Maretich P, and Kajimura S (2018). The Common and Distinct Features of Brown and Beige Adipocytes. Trends in endocrinology and metabolism: TEM 29, 191–200. [PubMed: 29366777]

Iwayama T, Steele C, Yao L, Dozmorov MG, Karamichos D, Wren JD, and Olson LE (2015). PDGFRalpha signaling drives adipose tissue fibrosis by targeting progenitor cell plasticity. Genes Dev 29, 1106–1119. [PubMed: 26019175]

Jiang Y, Berry DC, Jo A, Tang W, Arpke RW, Kyba M, and Graff JM (2017). A PPARgamma transcriptional cascade directs adipose progenitor cell-niche interaction and niche expansion. Nat Commun 8, 15926. [PubMed: 28649987]

Kajimura S, Spiegelman BM, and Seale P (2015). Brown and Beige Fat: Physiological Roles beyond Heat Generation. Cell Metab 22, 546–559. [PubMed: 26445512]

Kim JY, van de Wall E, Laplante M, Azzara A, Trujillo ME, Hofmann SM, Schraw T, Durand JL, Li H, Li G, et al. (2007). Obesity-associated improvements in metabolic profile through expansion of adipose tissue. J Clin Invest 117, 2621–2637. [PubMed: 17717599]

Klinghoffer RA, Mueting-Nelsen PF, Faerman A, Shani M, and Soriano P (2001). The two PDGF receptors maintain conserved signaling in vivo despite divergent embryological functions. Molecular cell 7, 343–354. [PubMed: 11239463]

Kranz A, Fu J, Duerschke K, Weidlich S, Naumann R, Stewart AF, and Anastassiadis K (2010). An improved Flp deleter mouse in C57Bl/6 based on Flpo recombinase. Genesis 48, 512–520. [PubMed: 20506501]

Kusminski CM, Bickel PE, and Scherer PE (2016). Targeting adipose tissue in the treatment of obesity-associated diabetes. Nature reviews Drug discovery 15, 639–660. [PubMed: 27256476]

Lao Z, Raju GP, Bai CB, and Joyner AL (2012). MASTR: a technique for mosaic mutant analysis with spatial and temporal control of recombination using conditional floxed alleles in mice. Cell reports 2, 386–396. [PubMed: 22884371]

Lee YH, Petkova AP, and Granneman JG (2013). Identification of an adipogenic niche for adipose tissue remodeling and restoration. Cell Metab 18, 355–367. [PubMed: 24011071]

Lee YH, Petkova AP, Konkar AA, and Granneman JG (2015). Cellular origins of cold- induced brown adipocytes in adult mice. FASEB J 29, 286–299. [PubMed: 25392270]

Lee YH, Petkova AP, Mottillo EP, and Granneman JG (2012). In vivo identification of bipotential adipocyte progenitors recruited by beta3-adrenoceptor activation and high-fat feeding. Cell Metab 15, 480–491. [PubMed: 22482730]

Lindahl P, Johansson BR, Leveen P, and Betsholtz C (1997). Pericyte loss and microaneurysm formation in PDGF-B-deficient mice. Science 277, 242–245. [PubMed: 9211853]

Madisen L, Garner AR, Shimaoka D, Chuong AS, Klapoetke NC, Li L, van der Bourg A, Niino Y, Egolf L, Monetti C, et al. (2015). Transgenic mice for intersectional targeting of neural sensors and effectors with high specificity and performance. Neuron 85, 942–958. [PubMed: 25741722]

Merrick D, Sakers A, Irgebay Z, Okada C, Calvert C, Morley MP, Percec I, and Seale P (2019). Identification of a mesenchymal progenitor cell hierarchy in adipose tissue. Science 364.

Nishimura S, Manabe I, Nagasaki M, Hosoya Y, Yamashita H, Fujita H, Ohsugi M, Tobe K, Kadowaki T, Nagai R, et al. (2007). Adipogenesis in obesity requires close interplay between differentiating adipocytes, stromal cells, and blood vessels. Diabetes 56, 1517–1526. [PubMed: 17389330]

Olson LE, and Soriano P (2009). Increased PDGFRalpha activation disrupts connective tissue development and drives systemic fibrosis. Dev Cell 16, 303–313. [PubMed: 19217431]

Olson LE, and Soriano P (2011). PDGFRbeta Signaling Regulates Mural Cell Plasticity and Inhibits Fat Development. Dev Cell 20, 815–826. [PubMed: 21664579]

Onogi Y, Wada T, Kamiya C, Inata K, Matsuzawa T, Inaba Y, Kimura K, Inoue H, Yamamoto S, Ishii Y, et al. (2017). PDGFRbeta Regulates Adipose Tissue Expansion and Glucose Metabolism via Vascular Remodeling in Diet-Induced Obesity. Diabetes 66, 1008–1021. [PubMed: 28122789]

Pontes-Quero S, Heredia L, Casquero-Garcia V, Fernandez-Chacon M, Luo W, Hermoso A, Bansal M, Garcia-Gonzalez I, Sanchez-Munoz MS, Perea JR, et al. (2017). Dual ifgMosaic: A Versatile

Method for Multispectral and Combinatorial Mosaic Gene-Function Analysis. Cell 170, 800–814 e818. [PubMed: 28802047]

Raymond CS, and Soriano P (2007). High-efficiency FLP and PhiC31 site-specific recombination in mammalian cells. PLoS One 2, e162. [PubMed: 17225864]

Ruzankina Y, Pinzon-Guzman C, Asare A, Ong T, Pontano L, Cotsarelis G, Zediak VP, Velez M, Bhandoola A, and Brown EJ (2007). Deletion of the developmentally essential gene ATR in adult mice leads to age-related phenotypes and stem cell loss. Cell Stem Cell 1, 113–126. [PubMed: 18371340]

Schmahl J, Rizzolo K, and Soriano P (2008). The PDGF signaling pathway controls multiple steroid-producing lineages. Genes Dev 22, 3255–3267. [PubMed: 19056881]

Schulz TJ, and Tseng YH (2013). Brown adipose tissue: development, metabolism and beyond. Biochem J 453, 167–178. [PubMed: 23805974]

Schwalie PC, Dong H, Zachara M, Russeil J, Alpern D, Akchiche N, Caprara C, Sun W , Schlaudraff KU, Soldati G, et al. (2018). A stromal cell population that inhibits adipogenesis in mammalian fat depots. Nature.

Shao M, Vishvanath L, Busbuso NC, Hepler C, Shan B, Sharma AX, Chen S, Yu X, An YA, Zhu Y, et al. (2018). De novo adipocyte differentiation from Pdgfrbeta(+) preadipocytes protects against pathologic visceral adipose expansion in obesity. Nat Commun 9, 890. [PubMed: 29497032]

Soriano P (1994). Abnormal kidney development and hematological disorders in PDGF beta-receptor mutant mice. Genes Dev 8, 1888–1896. [PubMed: 7958864]

Soriano P (1997). The PDGF alpha receptor is required for neural crest cell development and for normal patterning of the somites. Development 124, 2691–2700. [PubMed: 9226440]

Sun C, Berry WL, and Olson LE (2017). PDGFRalpha controls the balance of stromal and adipogenic cells during adipose tissue organogenesis. Development 144, 83–94. [PubMed: 28049691]

Tallquist MD, French WJ, and Soriano P (2003). Additive effects of PDGF receptor beta signaling pathways in vascular smooth muscle cell development. PLoS biology 1, E52. [PubMed: 14624252]

Tang W, Zeve D, Suh JM, Bosnakovski D, Kyba M, Hammer RE, Tallquist MD, and Graff JM (2008). White fat progenitor cells reside in the adipose vasculature. Science 322, 583–586. [PubMed: 18801968]

Vishvanath L, MacPherson KA, Hepler C, Wang QA, Shao M, Spurgin SB, Wang MY, Kusminski CM, Morley TS, and Gupta RK (2016). Pdgfrbeta+ Mural Preadipocytes Contribute to Adipocyte Hyperplasia Induced by High-Fat-Diet Feeding and Prolonged Cold Exposure in Adult Mice. Cell Metab 23, 350–359. [PubMed: 26626462]

Wang QA, Tao C, Gupta RK, and Scherer PE (2013). Tracking adipogenesis during white adipose tissue development, expansion and regeneration. Nat Med 19, 1338–1344. [PubMed: 23995282]

Xu T, and Rubin GM (2012). The effort to make mosaic analysis a household tool. Development 139, 4501–4503. [PubMed: 23172911]

Ye R, Wang QA, Tao C, Vishvanath L, Shao M, McDonald JG, Gupta RK, and Scherer PE (2015). Impact of tamoxifen on adipocyte lineage tracing: Inducer of adipogenesis and prolonged nuclear translocation of Cre recombinase. Molecular metabolism 4, 771–778. [PubMed: 26629402]

Zong H, Espinosa JS, Su HH, Muzumdar MD, and Luo L (2005). Mosaic analysis with double markers in mice. Cell 121, 479–492. [PubMed: 15882628]

HIGHLIGHTS

- Three new Pdgfra/Pdgfrb knockin mice for mosaic mutant analysis were made.
- Pdgfra- and Pdgfrb-lineages make distinct contributions to adipocyte differentiation
- Differentiation is transiently blocked by constitutive PDGFRα signaling
- Mosaic Pdgfra or Pdgfrb knockout enhances white/beige/brown adipogenesis

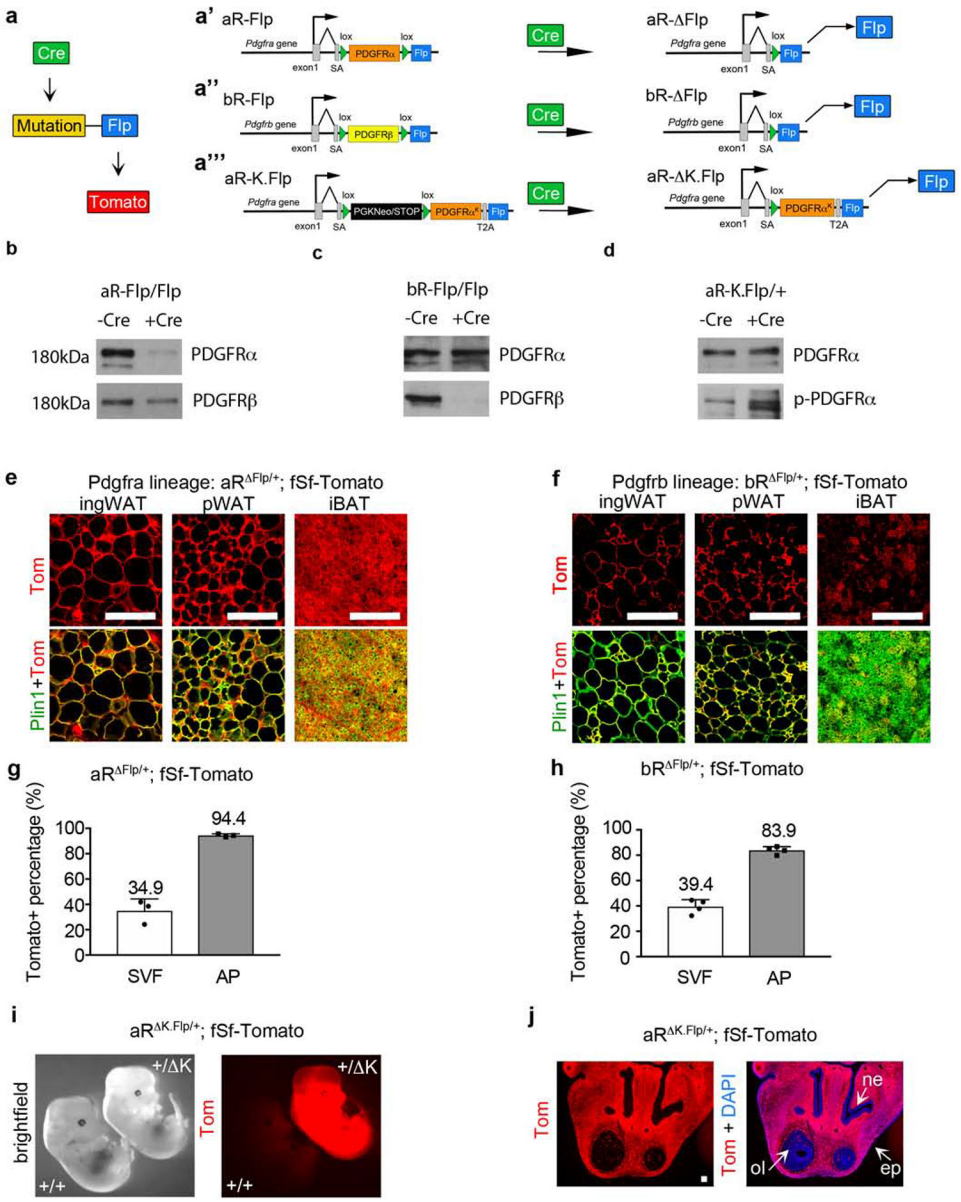

Figure 1. PDGFR-Flp mice create conditional *Pdgfra/Pdgfrb* mutations with genetically linked lineage tracing.

(a) The sequential dual-recombinase approach: Cre induces a mutation and Flp expression, and Flp induces Tomato expression. Flp is controlled by the endogenous *Pdgfra* or *Pdgfrb* promoters and is linked to a conditional *Pdgfr* mutation: **(a')** aR-Flp becomes aR-ΔFlp. **(a'')** bR-Flp becomes bR-ΔFlp. **(a''')** aR-K.Flp becomes aR-ΔK.Flp. **(b-d)** Primary dermal fibroblasts were infected with Cre-expressing lentivirus or -Cre control, followed by Western blot: **(b)** Blot from $aR^{Flp/Flp}$ cells, showing Cre-dependent deletion of PDGFRα. **(c)** Blot from $bR^{Flp/Flp}$ cells, showing Cre-dependent deletion of PDGFRβ. **(d)** Blot from $aR^{K.Flp/+}$ cells, showing Cre-dependent increased phosphorylation of PDGFRα. **(e** and **f)** Lineage tracing of embryonic *Pdgfra*- (**e**) or *Pdgfrb*- (**f**) lineages in inguinal WAT, perigonadal WAT, or interscapular BAT at P21, by immunofluorescence for Tomato and Perilipin-1. **(g** and **h)**

Flow cytometry of Tomato^{+} cells in the stromal vascular fraction (SVF) or adipocyte progenitor (AP) fraction at P21, with AP defined as Lin^{-} (CD31^{-} CD45^{-} Ter119^{-}), CD29^{+}, CD34^{+}. Tomato^{+} % in each fraction is shown + SD: (n = 3 or 4). **(i)** *aR*$^{+/+}$*;fSf-Tomato* or *aR*$^{\Delta K.Flp/+}$*;fSf-Tomato* embryos at E13.5. **(j)** Lineage tracing of the PDGFRα^{K}-lineage at E13.5 in the frontonasal prominence by Tomato epifluorescence with DAPI. Tomato is expressed in mesenchymal cells but is absent from epithelial and neuronal cells: nasal epilthelium (ne), olfactory lobe (ol) and epidermis (ep). All Scale bars: 100μm.
Detailed descriptions of the conditional alleles (**a'-a'''**) are shown in Supplementary Fig. 1.
Western blots from adult tissue and embryos are shown in Supplementary Fig. 2.
Absence of Tomato in Cre-naïve mice is shown in Supplementary Fig. 3.
Representative FACS plots and controls for **g** and **h** are shown in Supplementary Fig. 4.

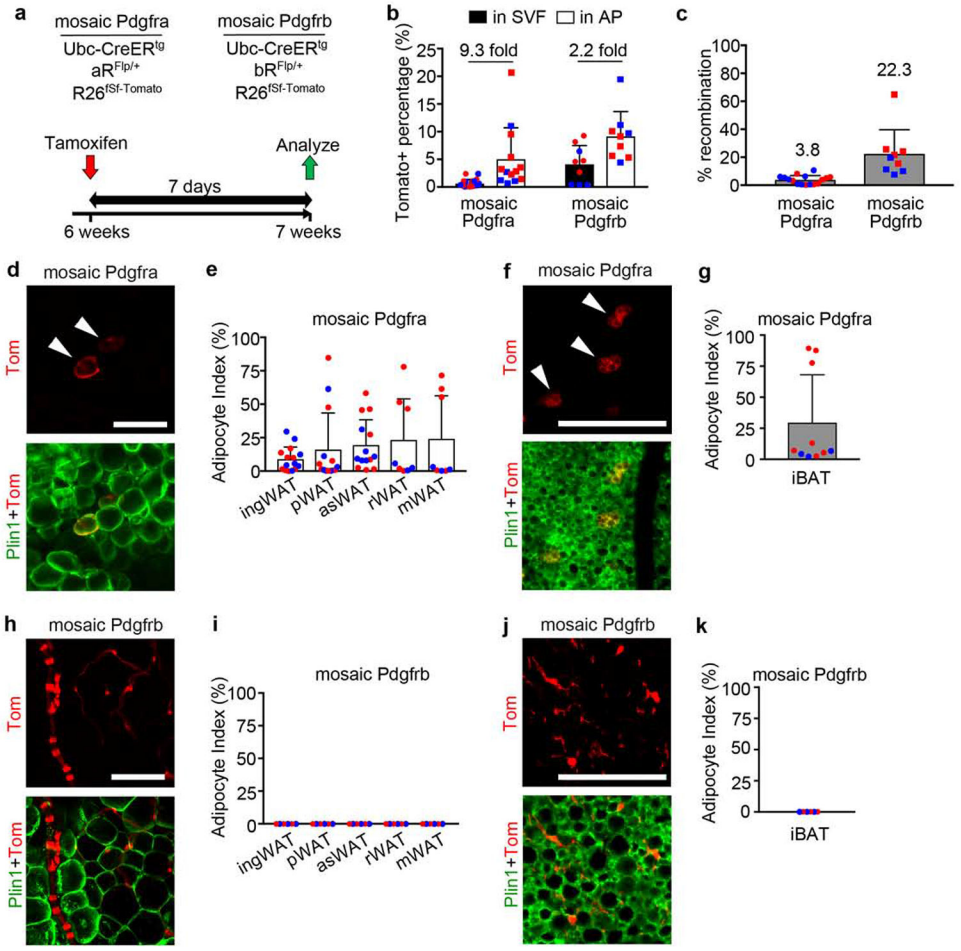

Figure 2. Short term adult mosaic labeling: *Pdgfra*-lineage labels adipocytes and *Pdgfrb*-lineage labels mural cells.

(a) Mosaic *Pdgfra* and *Pdgfrb* genotypes and experimental scheme for labeling induced at 6-weeks old with 1x Tmx (100mg/kg) and analysis after 7 days. (**b**) Flow cytometry of Tomato $^{+}$ cells in the SVF or AP fraction of ingWAT. Tomato^{+} % shown + SD, and fold enrichment of Tomato^{+} AP within Tomato^{+} SVF (n = 13 *Pdgfra,* 9 *Pdgfrb).* (**c**) qPCR for recombination efficiency in *Pdgfra* (n=13) or *Pdgfrb* (n=9) mosaics. Average recombination + SD. (**d-k**) Whole mount adipose tissue with Tomato lineage labeling and Plin1 immunofluorescence with quantification of adipocyte index + SD for each tissue. (**d**) *Pdgfra*-lineage labeling in ingWAT (arrowheads = WA). (**e**) Adipocyte index for mosaic *Pdgfra* WAT (n = 8-15). (**f**) *Pdgfra*-lineage labeling in iBAT (arrowheads = BA). (**g**) Adipocyte index for mosaic *Pdgfra* iBAT (n = 10). (**h**) *Pdgfrb*-lineage labeling in ingWAT (no WA labeling). (**i**) Zero adipocyte index for mosaic *Pdgfrb* WAT (n = 6). (**j**) *Pdgfrb*-lineage labeling in iBAT (no BA labeling). (**i**) Zero adipocyte index for mosaic *Pdgfrb* iBAT (n = 6). (**b,c,e,g,i,k**) Blue represents male and red represents female. All Scale bars: 100μm.

Histological controls for mosaic WAT/BAT and antibody stains for PDGFRa/PDGFRb are shown in Supplementary Fig. 5.

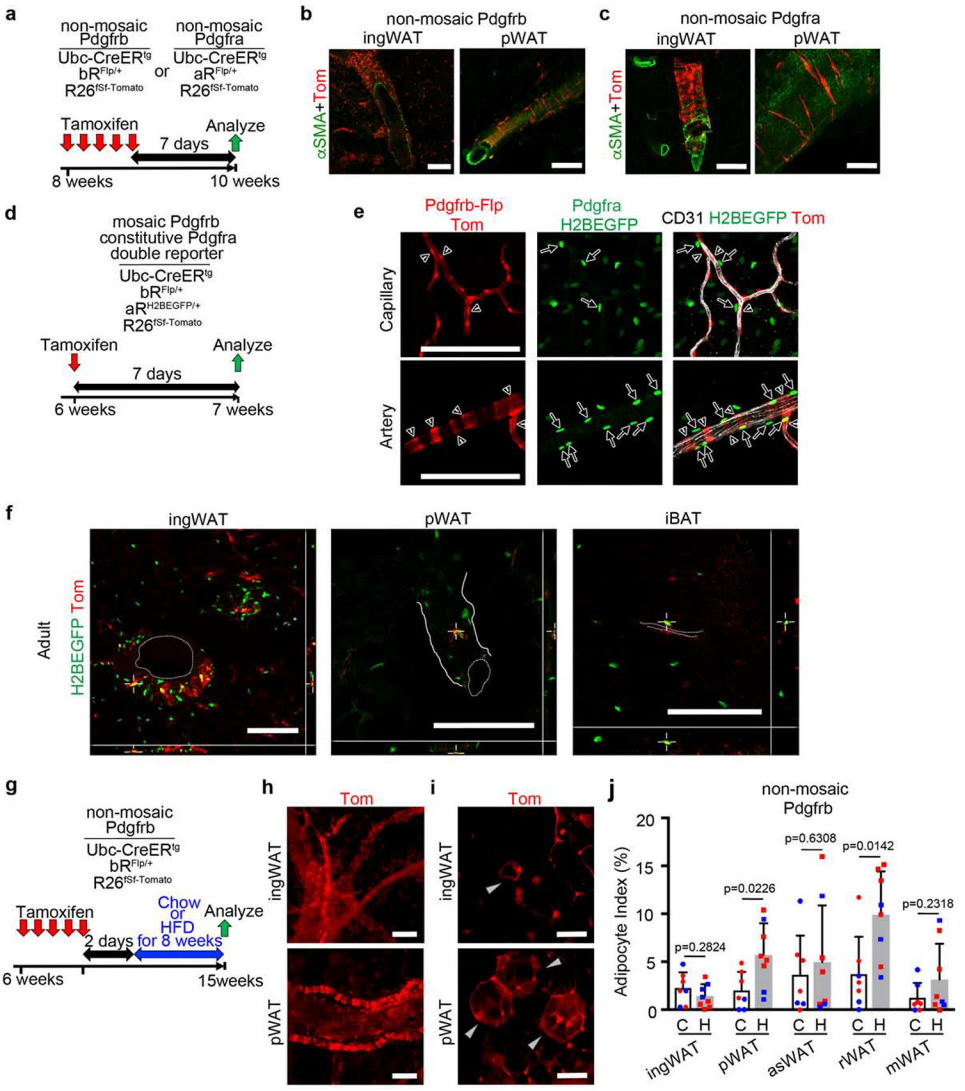

Figure 3. PDGFRα and PDGFRβ are expressed in the vascular adventitia under non-mosaic labeling conditions.

(**a**) Non-mosaic *Pdgfra* and *Pdgfrb* genotypes and experimental scheme for labeling at 8-weeks old with 5x Tmx (100mg/kg) and analysis after 7 more days. (**b** and **c**) Thick section WAT with Tomato labeling of adventitial fibroblasts and αSMA immunofluorescence of VSMCs. Representative of 1 male and 3 females (*Pdgfrb*) or 5 males and 6 females (*Pdgfra*). (**d**) Double reporter genotypes and experimental scheme for labeling at 6-weeks old with 1x Tmx (100mg/kg) and analysis after 7 days. (**e**) Thick section capillary or artery with *Pdgfrb*-lineage labeling (mural cells, red), PDGFRα$^+$ nuclei (green), and CD31 immunofluorescence (endothelial cells, white). Some GFP$^+$ cells are adjacent to blood vessels (arrows), but they are not co-labeled with Tomato$^+$ (arrowheads). Representative of 4 mice. (**f**) Confocal z-stack of rare adventitial fibroblasts co-labeled with PDGFRα-H2BGFP and *Pdgfrb*-lineage/Tomato. Dotted lines indicate vessel lumens and solid lines indicate perivascular outline. Representative of 3 male and 1 female. See also Supplementary Videos 1-3. (**g**) Non-mosaic *Pdgfrb* genotypes and experimental scheme for labeling at 6-weeks old

with 5x Tmx (100mg/kg) and analysis after 8 weeks of chow diet or HFD feeding. (**h-i**) Whole mount WAT with non-mosaic *Pdgfrb*-lineage/Tomato labeling of (**h**) adventitial fibroblasts or (**i**) adipocytes (gray arrowheads). (**j**) Adipocyte index + SD for non-mosaic *Pdgfrb* WAT after 8 weeks of chow diet (C) or HFD (H) (n = 7-8 mice). Blue represents male and red represents female. HFD differences are significant for pWAT and rWAT. All Scale bars: 100μm.

Additional data for HFD are shown in Supplementary Fig. 6.

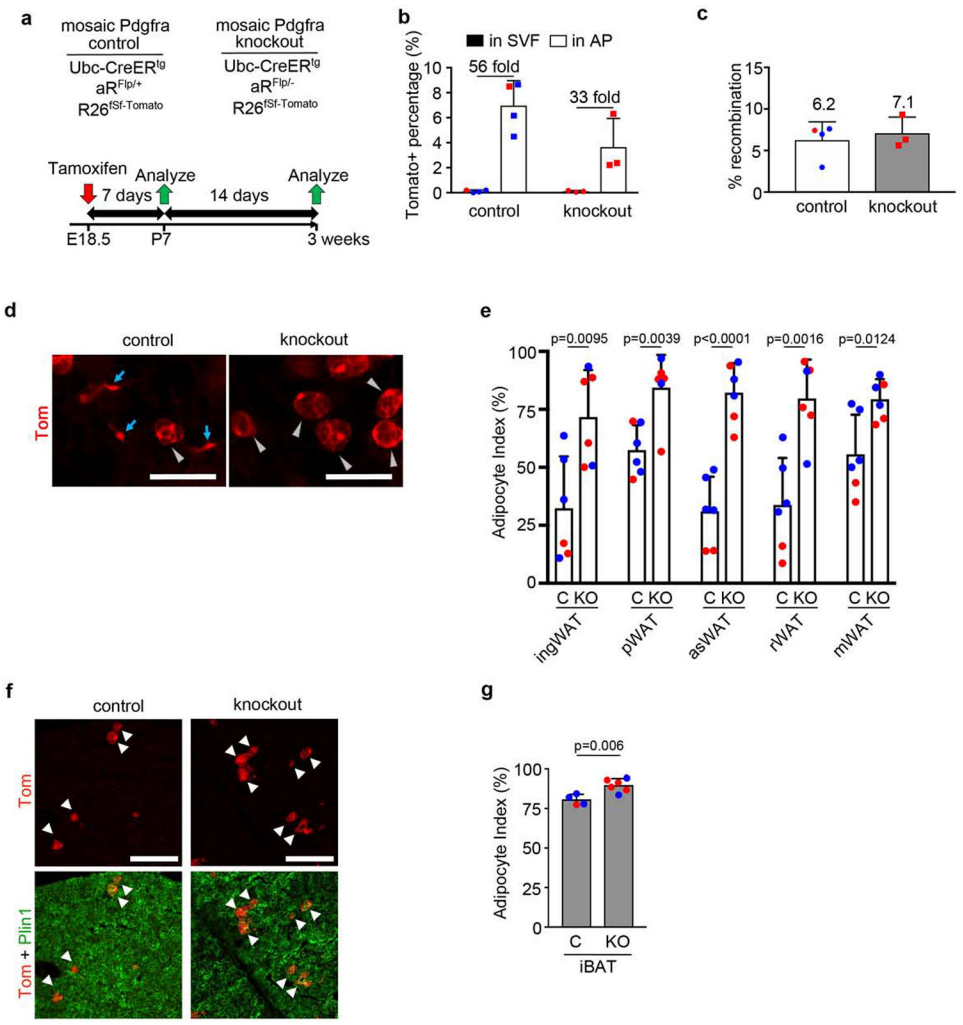

Figure 4. Mosaic inactivation of *Pdgfra* increases adipogenesis.

(**a**) Mosaic *Pdgfra* control or knockout genotypes and experimental scheme for labeling at E18.5 with 1x Tmx (50mg/kg) to pregnant dams, with analysis at P7 or P21. (**b**) Flow cytometry of Tomato$^+$ cells in the SVF or AP fraction of ingWAT at P7. Tomato$^+$ % shown + SD, and fold enrichment of Tomato$^+$ AP within Tomato$^+$ SVF (n = 3-4). (**c**) qPCR for recombination efficiency at P7. Average recombination + SD (n = 3-4). (**d**) Whole mount ingWAT at P21 with Tomato$^+$ stromal cells (blue arrows) and WA (gray arrowheads). (**e**) Adipocyte index + SD for mosaic *Pdgfra* control (C) or knockout (KO) WAT (n = 6). (**f**) iBAT at P21 with mosaic *Pdgfra* labeling in BA (arrowheads). (**g**) Adipocyte index + SD for mosaic *Pdgfra* control (C) or knockout (KO) iBAT (n = 4-6). (**b,c,e,g**) Blue represents male and red represents female. All scale bars: 100μm.

More description of the experimental scheme is shown in Supplementary Fig. 7.

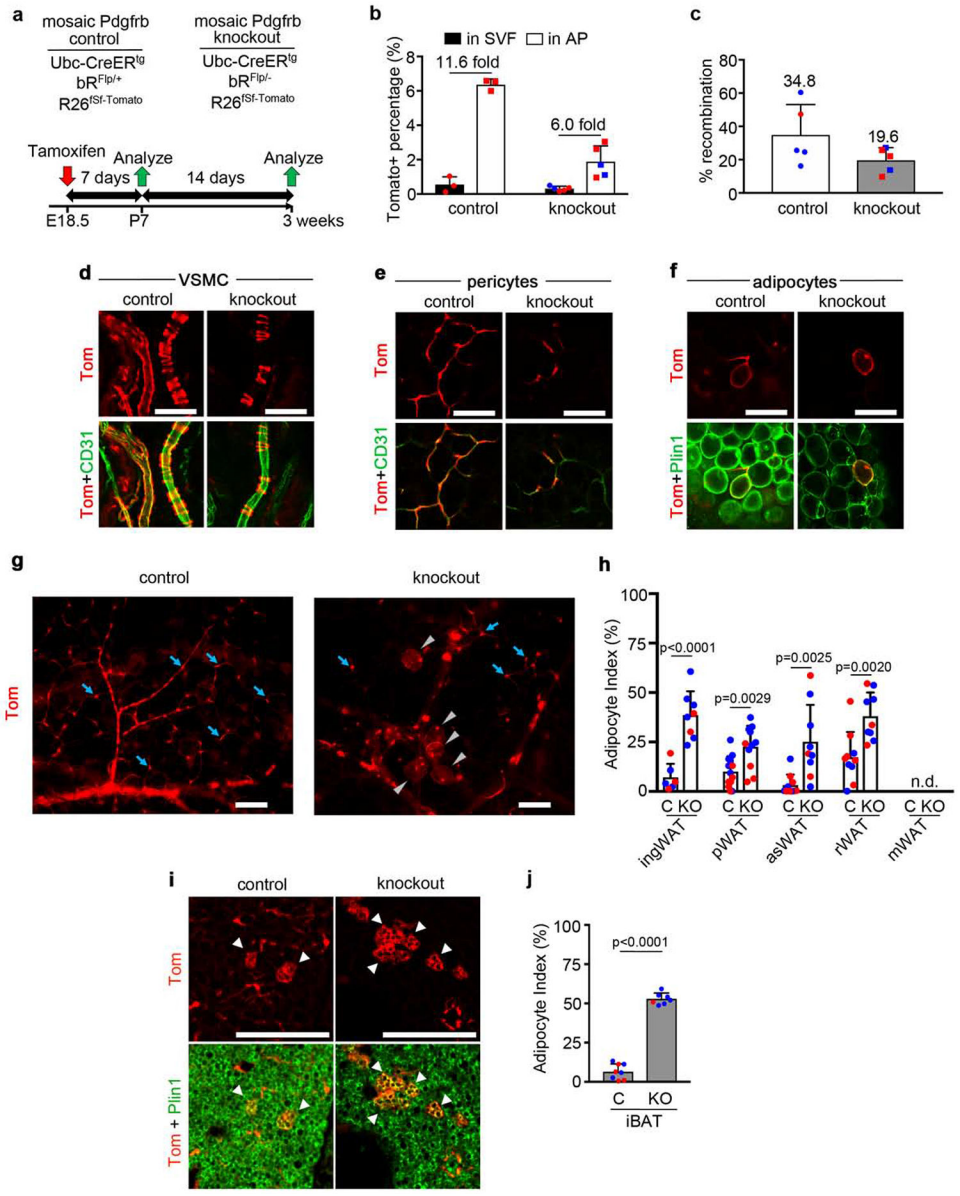

Figure 5. Mosaic inactivation of *Pdgfrb* increases adipogenesis.

(**a**) Mosaic *Pdgfrb* control and knockout genotypes and experimental scheme for labeling at E18.5 with 1x Tmx (50mg/kg) to pregnant dams, with analysis at P7. (**b**) Flow cytometry of Tomato$^+$ cells in the SVF or AP fraction of ingWAT at P7. Tomato$^+$ % in each fraction + SD, and fold enrichment of Tomato$^+$ AP within the Tomato$^+$ SVF (n = 3-5). (**c**) qPCR for recombination efficiency at P7. Average recombination + SD (n = 5). (**d-f**) Whole mount ingWAT at P21: (**d**) Tomato$^+$ vascular smooth muscle cells (VSMC) with CD31$^+$ endothelial cells (green). (**e**) Tomato$^+$ pericytes with CD31. (**f**) Tomato$^+$ WA with Plin1. (**g**) Whole mount ingWAT at P21 with Tomato$^+$ mural cells (blue arrows) and WA (gray arrowheads). (**h**) Adipocyte index + SD for mosaic *Pdgfrb* control (C) or knockout (KO) WAT (n = 6-11). mWAT was not analyzed. (**i**) iBAT at P21 with mosaic *Pdgfrb* labeling in BA (arrowheads).

(**j**) Adipocyte index + SD for mosaic *Pdgfrb* control (C) or knockout (KO) iBAT (n = 7-8). (**b,c,h,j**) Blue represents male and red represents female. All scale bars: 100μm. More description of the experimental scheme is shown in Supplementary Fig. 7.

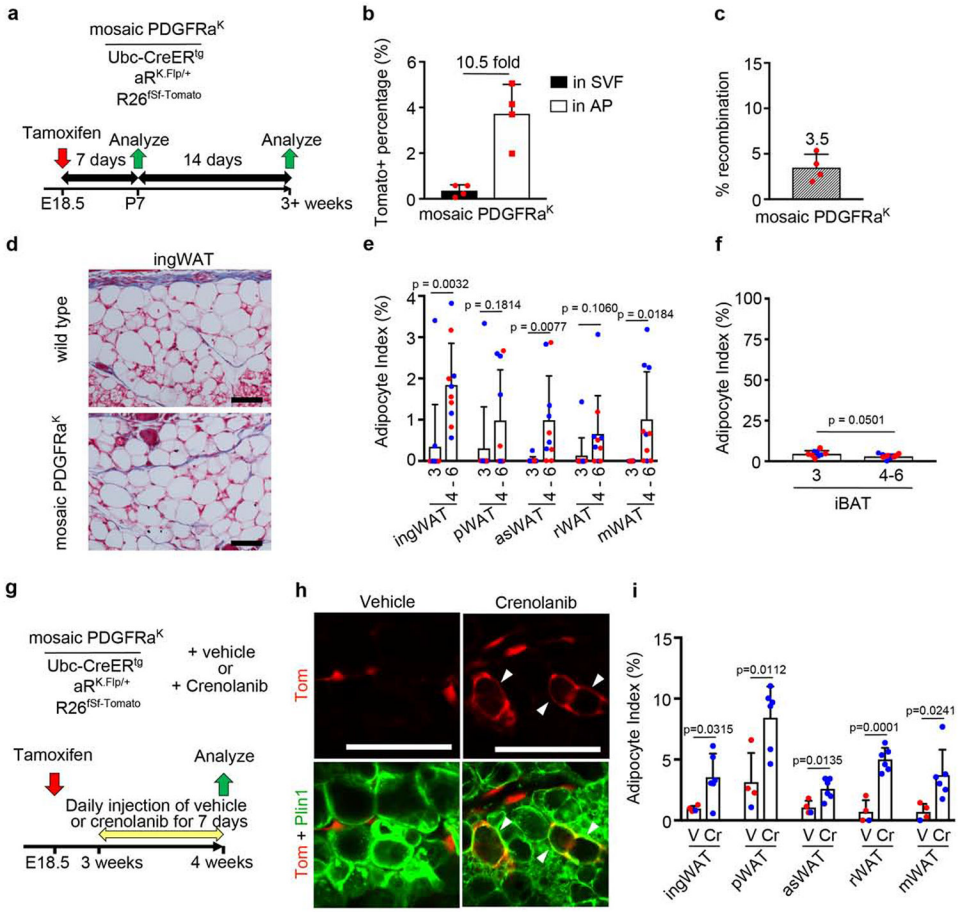

Figure 6. Mosaic constitutive PDGFRα^K signaling blocks adipogenesis and is reversible.

(**a**) Mosaic PDGFRα^K genotype and experimental scheme for labeling induced at E18.5 with 1x Tmx (10mg/kg) to pregnant dams, with analysis at P7 and P21 or later. (**b**) Flow cytometry of Tomato$^+$ cells in the SVF or AP fraction of ingWAT at P7. Tomato$^+$ % + SD, and fold enrichment of Tomato$^+$ AP within the Tomato$^+$ SVF (n = 4). (**c**) qPCR for recombination efficiency + SD (n = 4). (**d**) Trichrome-stained ingWAT from Tmx-treated wild type or mosaic PDGFRα^K littermate at P21, showing no evidence of fibrosis. (**e-f**) Adipocyte index + SD for mosaic PDGFRα^K WAT at P21 or 4-6 weeks. (**e**) Most WAT has adipocyte index of zero at 3 weeks, and a significantly higher index from 4-6 weeks. (**f**) iBAT adipocyte index decreases after 3 weeks (n = 6-10). (**g**) Mosaic PDGFRα^K genotype +/− crenolanib and experimental scheme for labeling at E18.5 with 1x 10mg/kg Tmx to pregnant dams. Vehicle or crenolanib were administered from 3 to 4 weeks, followed by analysis. (**h**) Whole mount ingWAT with mosaic PDGFRα^K labeling at 4 weeks. Tomato$^+$ WA (arrowheads) appear in crenolanib-treated mice. (**i**) Adipocyte index + SD for mosaic PDGFRα^K WAT treated with vehicle (V) or crenolanib (Cr) (n = 4-6). (**b,c,e,f,i**) Blue represents male and red represents female. All scale bars: 100μm.

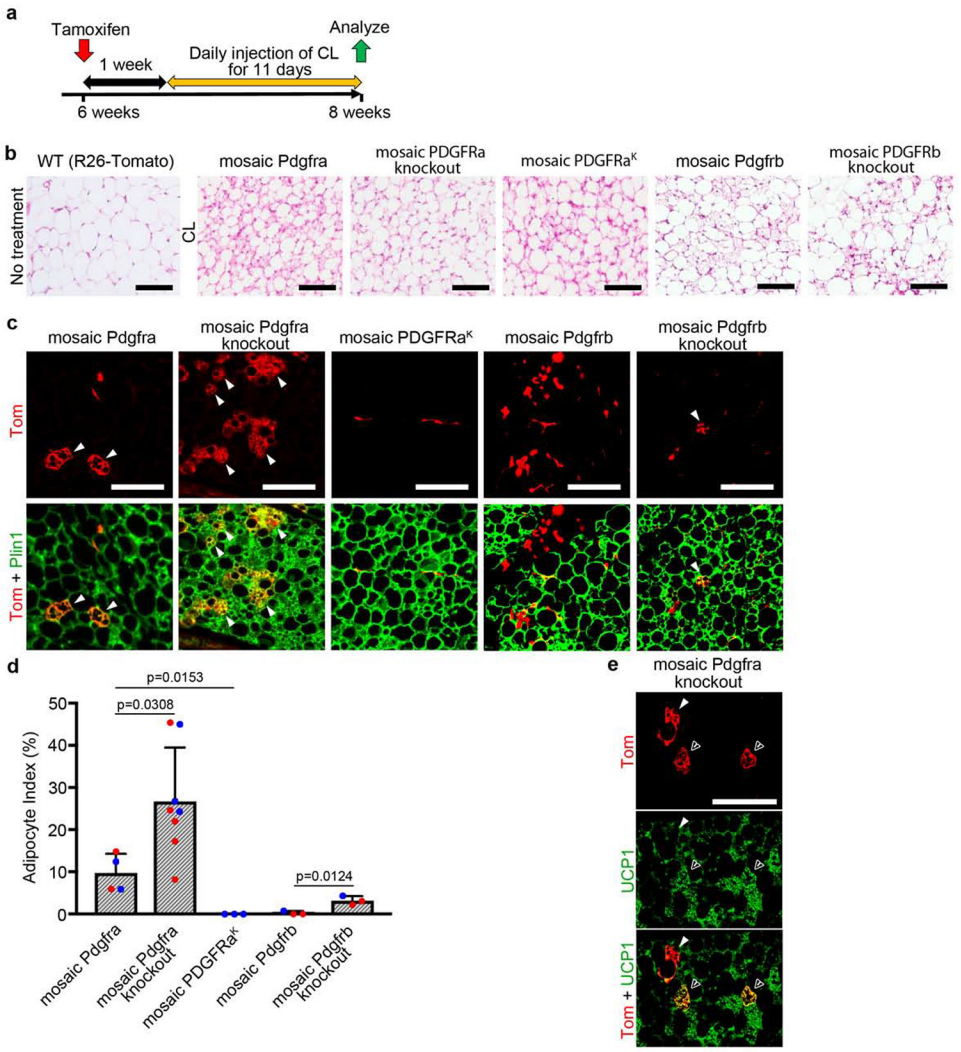

Figure 7. Mosaic inactivation of *Pdgfra/Pdgfrb* increases beige adipogenesis.

(**a**) Experimental scheme for labeling at 6 weeks with 1x Tmx, 1-week chase, 11 days of treatment with CL-316,243 (CL), and analysis at about 8 weeks. (**b**) H&E-stained pWAT without CL treatment, or different mosaic pWAT after 11-days CL showing browning response to Adrb3 activation. (**c**) Mosaic pWAT after CL treatment showing multilocular Tomato$^+$ beige adipocytes (bA) with Plin1 (arrowheads). Immunofluorescence on paraffin. (**d**) Beige adipocyte index + SD for mosaic pWAT after CL, which is the number of Tomato$^+$ bA divided by the total number of Tomato$^+$ cells counted (bA + WA + stromal) (n = 3-8). Blue represents male and red represents female. (**e**) Mosaic *Pdgfra* knockout pWAT after CL treatment, showing multilocular Tomato$^+$ bA with Ucp1 (open arrowhead) or without Ucp1 (filled arrowhead). All scale bars: 100μm.

KEY RESOURCES TABLE

REAGENT or RESOURCE	SOURCE	IDENTIFIER
Antibodies		
Rabbit monoclonal anti-Plin1	Cell Signaling	Cat# 9349
Rabbit polyclonal anti-UCP1	Abcam	Cat# 10983
Goat polyclonal anti-Plin1	Novus	Cat# 100-60554
Rabbit polyclonal anti-RFP	Rockland	Cat# 600-401-379
Armenian hamster polyclonal anti-CD31	Herzog 2013	Abcam #119341
Rabbit polyclonal anti-PDGFRα	Santa Cruz	Cat# 338
Goat polyclonal anti-PDGFRα	R&D	Cat# AF 1062
Rabbit polyclonal anti-PDGFRβ	Santa Cruz	Cat# 432
Rat monoclonal anti-PDGFRβ	eBioscience	Cat# 14-1402-82
Rabbit monoclonal anti-pY762 PDGFRα	Cell Signaling	Cat# 24188
Rabbit monoclonal anti-α-Smooth Muscle Actin	Cell Signaling	Cat# 19245
Donkey anti-rabbit HRP conjugate	Jackson ImmunoResearch	Cat# 711-035-152
Donkey anti-rabbit AF647 conjugate	Jackson ImmunoResearch	Cat# 711-605-152
Goat anti-Armenian hamster AF647 conjugate	Jackson ImmunoResearch	Cat# 127-605-099
Donkey anti-Goat AF488 conjugate	Jackson ImmunoResearch	Cat# 705-545-003
Donkey anti-Rabbit Cy3 conjugate	Jackson ImmunoResearch	Cat# 711-165-152
Donkey anti-Rabbit AF488 conjugate	Jackson ImmunoResearch	Cat# 711-545-152
Donkey anti-Rat AF488 conjugate	Jackson ImmunoResearch	Cat# 712-545-150
AF 700 anti-mouse/rat CD29	BioLegend	Cat# 102218
APC anti-mouse CD34	BioLegend	Cat# 119310
BV 421 anti-mouse CD45.2	BioLegend	Cat# 109831
PerCP/Cy5.5 anti-mouse CD31	BioLegend	Cat# 102420
PE/Cy7 anti-mouse TER-119/Erythroid Cells	BioLegend	Cat# 116221
Chemicals, Peptides, and Recombinant Proteins		
Tamoxifen (Tmx)	Sigma Aldrich	Cat# T5648
Crenolanib	Selleck Chemicals	Cat# S2730
CL316,243 (CL)	Cayman Chemical	Cat# 17499
Complete protease inhibitor cocktail	Sigma Aldrich	Cat# 11836170001
Collagenase Type 1	Gibco	Cat# 17100-017
Collagenase Type 2	Worthington	Cat# LS004176
DMEM	Corning	Cat# 10-017-CV
Fetal Bovine Serum	Atlanta Biologicals	S11550
L-glutamine	Gibco	25030
Pen/strep	Gibco	18140
Critical Commercial Assays		
ECL Western blotting substrate	Pierce	Cat# 32106

REAGENT or RESOURCE	SOURCE	IDENTIFIER
BCA assay	Pierce	Cat# 23225
iTaq SYBR Green Supermix	Bio-Rad	Cat# 1725122
Fluoro Gel with DABCO	Electron Microscopy Sciences	Cat# 17985-02
Zombie Green	BioLegend	Cat# 423111
DAPI	Sigma Aldrich	Cat# D9542
Masson's Trichrome Stain Kit	Electron Microscopy Sciences	Cat# 26367-series
Deposited Data		
Quantitative Datasets	This paper	doi:10.17632/26r263sm6w.1
Experimental Models: Organisms/Strains		
Mouse: Ubc-CreER^{tg}	Ruzankina 2007	JAX:007001
Mouse: Sox2-Cre^{tg}	Hayashi 2002	JAX:008454
Mouse: Pdgfra$^{H2B:GFP}$	Hamilton 2003	JAX:007669
Mouse: R26$^{LSL-fSf-tdTomato}$	Madisen 2015	JAX:021875
Mouse: Pdgfra^{floxed}	Tallquist & Soriano 2003	JAX:006492
Mouse: Pdgfrb^{floxed}	Schmahl 2008	JAX:010977
Mouse: Pdgfra$^{K.Flp}$	This paper	N/A
Mouse: Pdgfra^{Flp}	This paper	N/A
Mouse: Pdgfrb^{Flp}	This paper	N/A
Oligonucleotides		
aex2: ACCTCCCACCAGGTCTTTCT	This paper	N/A
ain2: CTGTAAGCCCATCCCAGAGA	This paper	N/A
aex3: GCCAGCTCACTTCACTCTCC	This paper	N/A
bex2: GGGCTTCCAGGAGTGATACC	This paper	N/A
bin2: CCAGCTGGACTGAAGAGGAG	This paper	N/A
bex3: CCGAGCAGGTCAGAACAAAG	This paper	N/A
SAF: CAAACTCTTCGCGGTCTTTC	This paper	N/A
aRR: CCCCATAGCTCCTGAGACCT	This paper	N/A
FlpR: CTTGCACAGGATGTCGAACTG	This paper	N/A
Flp1: GGCAGTTCGTGGAGAGATT	This paper	N/A
Flp2: GCCTTCTGGGTCTTGTACTT	This paper	N/A
Recombinant DNA		
pPGKPhiC31obpA	Raymond & Soriano 2007	Addgene Plasmid #13795
pFlpo	Raymond & Soriano 2007	Addgene Plasmid #13792
aR-K.Flp SA.lox.Neo/Stop.lox-PDGFRα^{K}.T2A.Flp targeting vector for the mouse **Pdgfra** gene	This paper	N/A
aR-Flp *sa-lox-Pdgfra-lox-Flp^{o}-attB-Neo-attP* targeting vector for the mouse *Pdgfra* gene	This paper	N/A
bR-Flp	This paper	N/A

REAGENT or RESOURCE	SOURCE	IDENTIFIER
sa-lox-Pdgfrb-lox-Flp^{o}-attB-Neo-attP targeting vector for the mouse *Pdgfrb* gene		
Lenti-mCMV/EF1alpha/HTLV-Cre-IRES-iRFP720-PGK-Puro	This paper	N/A
Lenti-mCMV/EF1alpha/HTLV-IRES-iRFP720-PGK-Puro	This paper	N/A
Software and Algorithms		
ImageJ	NIH	https://imagej.nih.gov/ij/
GraphPad Prism 7	GraphPad	https://www.graphpad.com/scientific-software/prism/
BD FACS Diva	BD Biosciences	https://www.bdbiosciences.com/enus/instruments/research-instruments/research-software/flow-cytometry-acquisition/facsdiva-software
FlowJo	FlowJo	https://www.flowjo.com/
NIS-Elements D3.2	Nikon	https://www.microscope.healthcare.nikon.com/products/software/nis-elements
NIS-Elements AR	Nikon	https://www.microscope.healthcare.nikon.com/products/software/nis-elements
ZEN	ZEISS	https://www.zeiss.com/microscopy/us/products/microscope-software/zen.html
Other		
LabDiet 5053 (normal chow)	Purina	LabDiet 5053
High Fat Diet (HFD)	Research Diets	D12492